

Planetary candidates transiting cool dwarf stars from Campaigns 12 to 15 of K2

A. Castro González¹, E. Díez Alonso^{1*}, J. Menéndez Blanco¹, John H. Livingston², Jerome P. de Leon², S. L. Suárez Gómez^{1,3}, C. González Gutiérrez¹, F. García Riesgo¹, L. Bonavera^{1,4}, F.J. Iglesias Rodríguez¹, R. Muñoz⁵, Mark E. Everett⁶, N. J. Scott⁷, Steve B. Howell⁷, David R. Ciardi⁸, Erica J. Gonzales^{9,10}, Joshua E. Schlieder¹¹, F. J. de Cos Juez¹

¹*Instituto Universitario de Ciencias y Tecnologías Espaciales de Asturias (ICTEA), C.Independencia 13, E-33004 Oviedo, Spain*

²*Department of Astronomy, University of Tokyo, 7-3-1 Hongo, Bunkyo-ku, Tokyo 113-0033, Japan*

³*Departamento de Matemáticas, Universidad de Oviedo, C. Federico García Lorca 18, E-33007, Oviedo, Spain*

⁴*Departamento de Física, Universidad de Oviedo, C.Federico García Lorca 18, E-33007, Oviedo, Spain*

⁵*Departamento de Informática, Universidad de Oviedo, Edificio Departamental 1. Campus de Viesques s/n, E-33204, Gijón, Spain*

⁶*NOIRLab, 950 N. Cherry Ave., Tucson, AZ 85719 USA*

⁷*NASA Ames Research Center, Moffett Field, CA 94035 USA*

⁸*NASA Exoplanet Science Institute-Caltech/IPAC 1200 E. California Blvd Pasadena, CA 91125*

⁹*Department of Astronomy and Astrophysics, University of California, Santa Cruz, 1156 High St. Santa Cruz, CA 95064, USA*

¹⁰*National Science Foundation Graduate Research Fellow*

¹¹*Exoplanets and Stellar Astrophysics Laboratory, Mail Code 667, NASA Goddard Space Flight Center, Greenbelt, MD 20771, USA*

Accepted 2020 July 24. Received 2020 June 26; in original form 2019 December 17

ABSTRACT

We analyzed the photometry of 20038 cool stars from campaigns 12, 13, 14 and 15 of the K2 mission in order to detect, characterize and validate new planetary candidates transiting low-mass stars. We present a catalogue of 25 new periodic transit-like signals in 22 stars, of which we computed the parameters of the stellar host for 19 stars and the planetary parameters for 21 signals. We acquired speckle and AO images, and also inspected archival Pan-STARRS1 images and Gaia DR2 to discard the presence of close stellar companions and to check possible transit dilutions due to nearby stars. False positive probability (FPP) was computed for 22 signals, obtaining $FPP < 1\%$ for 17. We consider 12 of them as statistically validated planets. One signal is a false positive and the remaining 12 signals are considered as planet candidates. 20 signals have orbital period $P_{\text{orb}} < 10 d$, 2 have $10 d < P_{\text{orb}} < 20 d$ and 3 have $P_{\text{orb}} > 20 d$. Regarding radii, 11 candidates and validated planets have computed radius $R < 2R_{\oplus}$, 9 have $2R_{\oplus} < R < 4R_{\oplus}$, and 1 has $R > 4R_{\oplus}$. 2 validated planets and 2 candidates are located in moderately bright stars ($m_{\text{kep}} < 13$) and 2 validated planets and 3 candidates have derived orbital radius within the habitable zone according to optimistic models. Of special interest is the validated warm super-Earth K2-323 b (EPIC 248616368 b) with $T_{\text{eq}} = 318_{-43}^{+24} K$, $S_p = 1.7 \pm 0.2 S_{\oplus}$, $R_p = 2.1 \pm 0.1 R_{\oplus}$, located in a $m_{\text{kep}} = 14.13$ star.

Key words: planets and satellites: detection – stars: low mass – techniques: photometric – methods: data analysis

1 INTRODUCTION

The Kepler mission (Borucki et al. 2010) was launched in 2009 with the scientific goal of exploring the structure and

* E-mail: diezalonso@uniovi.es

Table 1. Main features of studied campaigns.

Campaign	Start date	Stop date	Central coordinates	Area	Total number of stars	Investigated stars
12	December 15 th 2016	March 4 th 2017	$\alpha=23:26:38, \delta=-05:06:08$	South Galactic Cap	29362	4928
13	March 8 th 2017	May 27 th 2017	$\alpha=04:51:11, \delta=+20:57:11$	Hyades, Taurus - Auriga	21543	2186
14	May 31st 2017	August 19 th 2017	$\alpha=10:42:44, \delta=+06:51:06$	Leo and Sextant	30044	6256
15	August 23rd 2017	November 20 th 2017	$\alpha=15:34:28, \delta=-20:04:44$	Scorpius	23398	6668

diversity of planetary systems around main sequence stars. The satellite monitored ~ 150000 targets in a field located near the Galactic plane which is centered on Cygnus, Lyra and Draco. The main mission finished in 2013 with the loss of two reaction wheels, preventing the necessary pointing precision.

Between 2014 and 2018 the satellite kept operating on its second mission, *K2* (Howell et al. 2014), taking advantage of solar photon pressure to compensate for the lack of the reaction wheels. This new scenario implied the observation of fields located in the ecliptic plane. 19 fields were observed for temporal windows spanning ~ 80 days. In each campaign ~ 20000 targets were monitored in the standard long cadence mode of 29.5 minutes. Finally, running out of fuel, the satellite was retired on October 30th 2018.

Even though we are in the era of the Transiting Exoplanet Survey Satellite (TESS) (Ricker et al. 2014), which is expected to find thousands of transiting planets in bright nearby stars, Kepler has been the most successful instrument in detecting planetary candidates. As of June 2020, 2341 confirmed and 2418 candidate planets have been detected during its prime mission (e.g. Borucki et al. 2011; Batalha et al. 2013; Burke et al. 2014) and 409 confirmed and 889 candidates during its extended mission (e.g. Vanderburg et al. 2015; Crossfield et al. 2016; Livingston et al. 2018a,b; Díez Alonso et al. 2018a,b, 2019). Despite the large amount of confirmed and candidate planets detected by the Kepler’s first and second mission, a lot of planetary signals still remain undetected, waiting to be identified for future confirmation and characterization.

Our understanding of planetary systems has totally changed due to satellite discoveries, with the high occurrence rate of small planets ($R_p < 4R_{\oplus}$) around low-mass stars one of its most important results (Howard et al. 2012; Dressing & Charbonneau 2013, 2015; Mulders et al. 2015a,b).

Low-mass stars ($0.1 M_{\odot} < M < 0.6 M_{\odot}$) account for 70% of the stellar population in the Galaxy (Henry et al. 2006), so they have a significant impact on the overall statistics of planets. The advantages of detection are multiple for these stars as well. First, as the dimming in brightness due to transits is proportional to the planet - stellar radius ratio (R_p/R_*)² (Mandel & Agol 2002), transiting planets orbiting around these stars are easier to detect. Second, low-mass stars are more suitable for radial velocity follow-up, favoring the confirmation of their planets and mass measurements. Third, the signal amplitude in transmission spectroscopy is higher (Charbonneau et al. 2002), so planets orbiting around cool stars are good targets for atmospheric characterization. Also, habitable zones (HZ) around these cool stars are closer, facilitating the detection and characterization of planets in the habitable zone. In this paper we present the results of our search of planetary candidates transiting low-mass stars from campaigns 12, 13, 14 and 15 of *K2*, with 23 new transit-

like signals in 21 low-mass stars and 2 signals in an early K-type dwarf star, of which 12 were statistically validated as planets, 1 is a false positive and 12 remain as candidates. In Section 2 we describe the selection process of the researched stars and the methodology to detect planetary candidate signals. In Section 3 we describe the procedure followed in order to obtain the stellar parameters of the planetary candidate hosts, and also the data acquisition and analysis of the speckle and AO images. In Section 4 we describe how we obtained the parameters of planetary candidates and the studied validation indicators. In Section 5 we discuss the results obtained, while the conclusions of the work are summarized in Section 6.

2 SELECTION OF TARGET STARS AND SEARCHING FOR PLANETARY CANDIDATES

Our search focused on cool stars from campaigns 12, 13, 14 and 15 of *K2*, which were the last four public campaigns at the time of doing the analysis. Previous campaigns have been studied to inform the community about planetary candidates (e.g. Pope et al. 2016; Vanderburg et al. 2016; David et al. 2018; Yu et al. 2018; Kruse et al. 2019) but, although various planets have been confirmed in campaigns 12 to 15 (e.g. Gillon et al. 2017; Díez Alonso et al. 2018a; David et al. 2018; Díez Alonso et al. 2018b, 2019), according to the *NASA Exoplanet Archive*¹, only 13 candidates have been published in these campaigns by Zink et al. (2019) (8 from C12 and 5 from C13. See Figure 2). Table 1 summarizes the main features of each campaign (start and stop observing dates, central coordinates of each field, sky region, number of monitored targets by *K2* and the number of selected and studied cool stars in this work).

To select cool stars we started from the *Ecliptic Plane Input Catalog (EPIC)* (Huber et al. 2016), which provides coordinates, photometry and kinematics for all the *K2* targets, based on multiple all-sky catalogues. The catalogue also provides stellar properties (temperatures, radii, masses, surface gravities, metallicities, densities, distances and extinctions) computed from colours, proper motions, spectroscopy and stellar population models. For the cross-matching process we used the online query tool available at the *Mikulski Archive for Space Telescopes (MAST)*².

With a precision of $\sim 2-3\%$ in T_{eff} , the EPIC catalogue misclassifies 56 – 72% of subgiants as dwarfs, and 9% of dwarfs as subgiants (Huber et al. 2016). It also underestimates radii for M dwarfs up to 20%, as it relies on

¹ <https://exoplanetarchive.ipac.caltech.edu/index.html>

² <https://archive.stsci.edu/k2/epic/search.php>

Padova stellar models (Marigo et al. 2008) with systematically smaller radii for M dwarfs. For these reasons, in the selection process we only imposed the condition $T_{\text{eff}} < 4100$ K to obtain a set of M and late K-type stars. Later, we obtained independent and more accurate stellar parameters than those collected in EPIC for all the stars with promising transit-like signals presented in this work (see Section 3 and Table A2). The selection process resulted in 6668 cool stars from campaign 15, 6256 from campaign 14, 2186 from campaign 13 and 4928 from campaign 12 (total amount of 20038 selected cool stars).

We downloaded from MAST³ the K2 Self Flat Fielding (K2SFF) corrected light curves for all the stars of our sample. The K2SFF pipeline (Vanderburg & Johnson 2014) eliminates most of the systematic photometric errors caused by the spacecraft drift during the K2 mission. The photometry of the 20038 filtered stars was analysed with the `lctools` software (Schmitt et al. 2019) to search for planetary transit-like signals. The software performs a moving median detrending process, after which the *BLS* (*Box-fitting Least Squares*) algorithm (Kovács et al. 2016) is applied in order to find periodic dips that may have been caused by planetary transits. With an imposed lower value of $\text{SNR} = 6$ for the signal-to-noise ratio of candidate signals (computed from equation 14 of Hartman & Bakos 2016), and constrained to find a maximum of 3 different signals per light curve, `lctools` detected a total of 13309 signals in the four studied campaigns, resulting in a mean value of ~ 0.66 signals per star. Figure 1 shows an example of the corrected K2SFF photometry for a star from this work (K2-322, EPIC 248558190) showing clear modulations due to stellar rotation, along with the normalized light curve after removing the stellar variability. The dips due to the validated planet K2-322 b can be easily seen (highlighted in green). This target also shows the presence of a single transit event (highlighted in blue), most likely due to a long period planet (see individual discussion in Section 5).

All signals were visually inspected to reject those with obvious non-transit origin. Spurious signals were those most commonly discarded. Furthermore stellar rotations, characterized by periodic modulations with periods ranging from hours to multiple days, eclipsing binaries, with clear primary and secondary minima and showing depths typically deeper than transits ($\geq 1\%$), and irregular variable stars. While performing the visual inspection, we also excluded transit-like signals with less than three transits in the K2 light curve, so candidates with orbital periods longer than half the temporal spanning of the campaigns (~ 40 days) were omitted from this work. However, these candidates are being studied for a specific follow-up.

After the cleaning process, we finished with a list of 25 new promising candidate signals in 22 stars (see Section 5, and Tables A2 and A3). Furthermore, among the previous published confirmed and candidate systems belonging to the four studied campaigns (30 confirmed and 12 candidates), 8 of them (7 confirmed and 1 candidate) satisfies the selection condition $T_{\text{eff}} < 4100$ K adopted in this work. These 8 systems were also detected, showing the completeness of our signal search and the posterior vetting.

³ <https://archive.stsci.edu/hlsp/k2sff>

3 STELLAR CHARACTERIZATION OF PLANET CANDIDATE HOSTS

3.1 Stellar parameters

To obtain the stellar parameters (radii, masses, effective temperatures and surface gravities) for the stars of our final list of candidate hosts, we used the `isochrones` package⁴, an interpolation tool for the fitting of stellar models to photometric or spectroscopic parameters (Morton 2015). The software does trilinear interpolation in mass-age-[Fe/H] space for any given set of model grids, thus being able to predict the value for any physical or photometric property derived by the models. The package uses the MESA Isochrones Stellar Tracks (MIST) models (Paxton et al. 2015; Dotter 2016; Choi et al. 2016), which are included in the `isochrones` package. These models are computed with the Modules for Experiments in Stellar Astrophysics (MESA) code (Paxton et al. 2011). The current MIST release consists of masses ranging from 0.1 to 300 M_{\odot} , $\log(\text{age})$ ranging from 5 to 10.3, and solar-scaled abundances adopted from Asplund et al. (2009), with metallicities ranging from $[\text{Fe}/\text{H}] = -4$ to 0.5. We acquired parallaxes and their uncertainties from Gaia DR2 (Gaia Collaboration et al. 2018) and the wide band *BVHJKgri* photometry and their uncertainties from the EPIC catalogue⁵ (see Table A1). Comparing with the EPIC catalogue, the isochrones-derived T_{eff} can be estimated to within 8% for the cool stars of our sample, considering the difference as:

$$\frac{\|T_{\text{EPIC}} - T_{\text{isochrones}}\|}{\|T_{\text{EPIC}}\|} \quad (1)$$

which results in a value of 0.08062 relative error. Although straightforward, the use of this error makes it possible to give a general measure of the difference of both estimations, adjusted in consideration of the EPIC values.

The `isochrones`-derived parameters are model-dependent, so when available, they should be replaced by those obtained by asteroseismology or spectroscopy. Regarding uncertainties, we note that some of them are well below 1% in T_{eff} and $\sim 1\%$ in mass and radius, which are not creditable. We emphasize that these tabulated uncertainties only take into account the measurement error from the observations and the dispersion due to the MCMC analysis, and not the inherent uncertainties in the models themselves, so therefore they may be underestimated.

It is worth to mention that 4 stars characterized with `isochrones` have a final estimated effective temperature $T_{\text{eff}} > 4100$ K, the highest T_{eff} imposed to cross match the EPIC catalogue. The final adopted stellar parameters and their uncertainties are presented in Table A2.

Two stars (EPIC 201663913⁶ and K2-325) have been characterized from acquired spectra by Dressing et al. (2019). In both cases, the published stellar parameters were adopted instead of those derived with `isochrones`.

⁴ <https://github.com/timothydmorton/isochrones>

⁵ EPIC catalogue adopts *gri* photometry from SDSS (Sloan Digital Sky Survey) DR9 (Ahn et al. 2012). In cases where it is not available, we adopted *gri* photometry from SDSS DR15 (Aguado et al. 2019) or Pan-STARRS DR1 (Flewelling 2018).

⁶ Posterior analysis showed that the signals present at EPIC 201663913 are a contamination from EPIC 201663879.

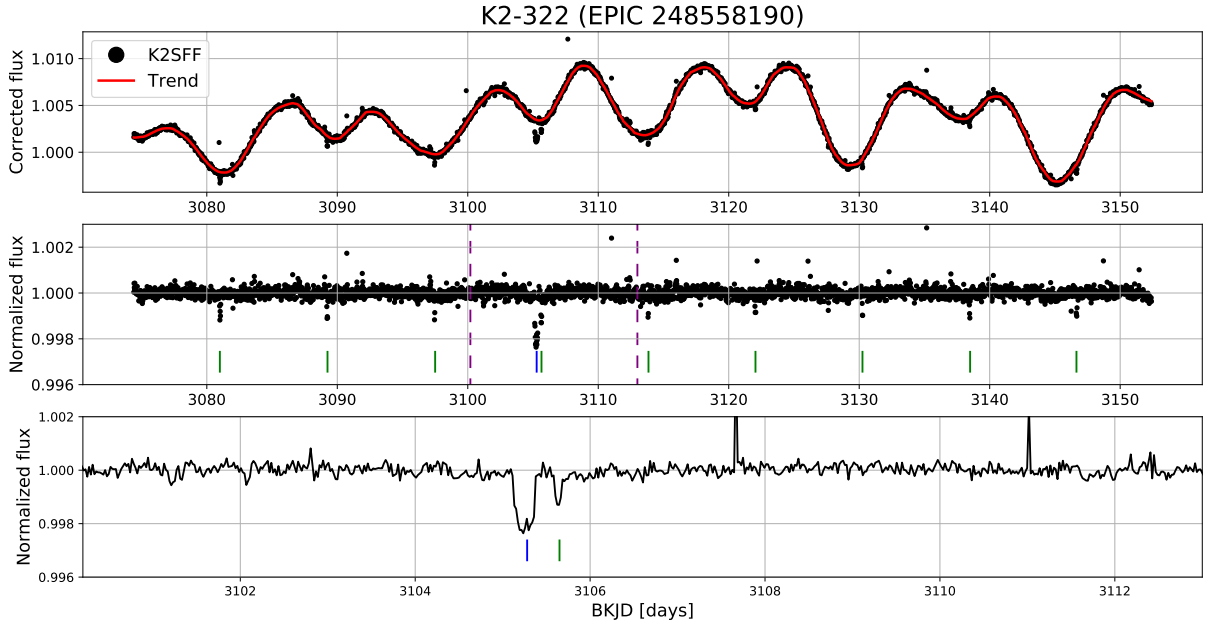


Figure 1. K2 long cadence photometry of the star K2-322. Top: K2SFF photometry after removal of telescope systematics, revealing a clear rotation modulation, along with the trend line (in red) corresponding to a moving median of 1.5-day boxcar size (72 data points). Mid: detrended light curve showing the location of the 8.2-day periodic dips of the validated planet K2-322 b (green lines). The location of a single transit event, most likely due to another planet in the system is also highlighted (blue line). Bottom: zoom in (within the vertical dashed lines) over the normalized light curve showing more clearly the single transit event along with a transit of the validated planet K2-322 b.

We also checked our stellar parameters comparing with those recently published in [Hardegree-Ullman et al. \(2020\)](#), which provides significant improvement over EPIC catalogue due to added spectroscopic constraints. The comparison indicates a good agreement, computing a 4.7% relative error for the stellar radii, in contrast with the 43% relative error when comparing with EPIC. The radii discrepancy with EPIC is also consistent with [Dressing et al. \(2019\)](#), where it was computed $\sim 40\%$.

3.2 Speckle and IR/AO imaging and identification of nearby contaminating stars

We acquired speckle and AO images for 11 stars⁷ of our final sample to rule out the presence of close or blended sources. Not only could close sources imply a misidentification in the origin of the signal, but also the stellar characterization with *isochrones* may be unreliable due to photometric contamination between both sources. We also inspected Pan-STARRS1 ([Chambers et al. 2016](#)) images of the 22 stars to discard close or blended sources.

The speckle images were acquired with the NESSI instrument at the 3.5 m WIYN telescope (Kitt Peak, Arizona) and DSSI at the 8 m GeminiS telescope (Cerro Pachón,

Chile). The AO images were acquired with NIRC2 at the 10 m Keck telescope (Maunakea, Hawaii).

NESSI ([Scott et al. 2018](#)) is a dual-channel imager using high-speed readout EMCCD detectors and a dichroic to split optical light at ~ 700 nm. Speckle images are obtained in a shutterless stream of 1000 images per set, each image being 40 ms in duration. Depending on the target brightness, 1-3 or more sets are obtained in a row, each providing a blue and red image. All of the observations presented here used a blue filter having central wavelength/bandpass values of 562/44 nm and a 832/40 nm red filter. The data files are passed through our standard Fourier analysis pipeline ([Horch et al. 2009](#)) in which the average power spectrum for each image is computed and summed. We next deconvolve the speckle transfer function through division by the power spectrum of a point source standard star (taken spatially and temporally close to the target star) and compute a weighted least-square fit of a fringe pattern to the result. During this step, pixels in the Fourier plane that have low signal-to-noise and low-frequency values judged to be in the seeing disk are set to zero. In order to determine the highest probability quadrant location of the companion star, we compute a reconstructed image via bispectral analysis ([Lohmann et al. 1983](#)). Resolved star systems produce a characteristic interferometric fringe pattern from which the separation, position angle, and delta magnitude can be determined through a modeling procedure. Details of our data reduction techniques and error assessments are given in [Horch et al. \(2011\)](#) and [Howell et al. \(2011\)](#).

⁷ All the images are available at ExoFOP-K2 <https://exofop.ipac.caltech.edu/k2/>

The Differential Speckle Survey Instrument (DSSI; Horch et al. 2009) was installed as a visitor instrument on the Gemini South 8m telescope during a run of 6 nights during 2018 March and April. DSSI employs two high-speed EMCCD cameras to obtain simultaneous optical speckle image sets in two filters for diffraction-limited spatial resolution. Speckle image reconstruction is used to detect or constrain the presence of any additional sources within $\approx 1''$ of a target star. Each target star was observed with filters having central wavelength/bandpass values of 692/40 nm and 880/50 nm. The star was centered in a 256×256 pixel ($2.8'' \times 2.8''$) window of each detector. The data consisted of sets of images, where each set is a data cube of 1000 frames with frame exposure times of 60 ms. Along with each science target, a nearby, bright ($V \approx 5$) calibrator star was observed with one 1000-frame data set. These calibration stars were chosen to be single stars, in order to represent the instrumental PSF of the speckle data (their point source nature is confirmed during data reduction).

The data were reduced as described in Howell et al. (2011) to produce a set of high-level data products. These include, for each filter, a reconstructed (diffraction-limited) image of the field surrounding each target star and a contrast curve giving the relative limiting magnitude of any undetected point source as a function of angular separation from the target. Briefly, to construct the images, the autocorrelation function of each frame is calculated, then co-added over the image set. These are transformed into power spectra, and the power spectrum of each science target is divided by that of its point source to find the modulus of the power spectrum of the science target. A set of bispectral subplanes are also found for each image set and used according to the algorithm of Meng et al. (1990) to provide phase information that, when combined with the power spectrum modulus, correct the phase of the image. The result is filtered with a Gaussian having a FWHM corresponding to the diffraction limit of the telescope and this is then inverse-transformed to produce the reconstructed image.

The contrast curves are measured from the reconstructed images by measuring, within a set of concentric annuli centered on the target star, the standard deviation, σ , of local minima and maxima in the image background. These local minima and maxima are effectively the noise threshold against which the signal (i.e. peak) of any neighboring star must be detected. The contrast curve is defined based on a smoothed fit over the 5σ values from each annulus with magnitude differences measured relative to the peak of the target star.

The Keck Observatory observations were made with the NIRC2 instrument on Keck-II behind the natural guide star AO system. The observations were made on 2018 Nov 22 UT in the standard 3-point dither pattern that is used with NIRC2 to avoid the left lower quadrant of the detector which is typically noisier than the other three quadrants. The dither pattern step size was $3''$ and was repeated twice, with each dither offset from the previous dither by $0.5''$. The observations were made in the narrow-band $Br-\gamma$ filter ($\lambda_o = 2.1686$; $\Delta\lambda = 0.0326 \mu\text{m}$) with an integration time of 10 seconds with one coadd per frame for a total of 90 seconds on target. The camera was in the narrow-angle mode with a full field of view of $\sim 10''$ and a pixel scale of approximately $0.099442''$ per pixel.

The AO data were processed and analyzed with a custom set of IDL tools. The science frames were flat-fielded and sky-subtracted. The flat fields were generated from a median average of dark subtracted flats taken on-sky. The flats were normalized such that the median value of the flats is unity. The sky frames were generated from the median average of the dithered science frames; each science image was then sky-subtracted and flat-fielded. The reduced science frames were combined into a single combined image using an intra-pixel interpolation that conserves flux, shifts the individual dithered frames by the appropriate fractional pixels, and median-coadds the frames. The final resolution of the combined dither was determined from the full-width half-maximum of the point spread function; $0.059''$.

The sensitivities of the final combined AO image were determined by injecting simulated sources azimuthally around the primary target every 45° at separations of integer multiples of the central source's FWHM (Furlan et al. 2017). The brightness of each injected source was scaled until standard aperture photometry detected it with 5σ significance. The resulting brightness of the injected sources relative to the target set the contrast limits at that injection location. The final 5σ limit at each separation was determined from the average of all of the determined limits at that separation and the uncertainty on the limit was set by the rms dispersion of the azimuthal slices at a given radial distance.

The speckle and AO images rule out the presence of close companions except for EPIC 250001426 and EPIC 246163416, which have a secondary source situated at $0.23''$ and $0.65''$ respectively. Also, analysis of the Pan-STARRS1 images for the stars without speckle or AO images rule out the presence of close companions with $\Delta\text{mag} < 5$ at angular separation $> 2.5''$, with the exception of EPIC 245944983 (a binary star with angular separation of $4''$ between components), EPIC 246331418 (also a binary star with the secondary component at angular separation of $3''$) and EPIC 249391469, with a faint source with angular separation of $5.85''$ (see individual discussion in Section 5 for more details).

In Table 3 we summarize the 25 signals belonging to the 22 stars, for which the limits on the presence of nearby stars have been obtained by speckle, AO or archival Pan-STARRS1 images. All the speckle images, with their extracted contrast curves, and the images from Pan-STARRS1, are presented in Appendix A (Figures A4 and A5, Figures A6 to A9 respectively) and discussed in Sections 4 and 5.

Five stars showing transit-like signals have radial velocity measurements from Gaia DR2 (summarized in Table 2). From the radial velocities, distances, proper motions and coordinates of these five stars, we checked their membership to any moving group from Malo et al. (2013), using the code from Rodriguez (2016), finding no matches.

Table 2. Proper motions and radial velocities for the five stars of our sample with V_r available from Gaia DR2. Distances from Gaia DR2 for the entire sample are listed in Table A2.

EPIC	μ_α [mas/yr]	μ_δ [mas/yr]	V_r [km/s]
201663879	-2.85 ± 0.07	-22.73 ± 0.05	8.63 ± 1.83
245944983	109.47 ± 0.05	25.50 ± 0.03	25.38 ± 1.70
248480671	50.92 ± 0.07	-109.19 ± 0.06	-43.89 ± 0.89
248558190	-16.30 ± 0.04	-2.64 ± 0.03	4.18 ± 1.42
248782482	107.70 ± 0.07	-38.22 ± 0.06	-4.21 ± 1.26

4 CANDIDATES CHARACTERIZATION AND STATISTICAL VALIDATION

We used the `pyaneti` package⁸ (Barragán et al. 2019) to characterize the planetary candidates. The code uses a Bayesian approach combined with an MCMC sampling to infer the candidate parameters. From the phase-folded light curve of the transit, the orbital period, the computed stellar mass, radius and effective temperature as fixed parameters, and the orbital radius, planet radius and the quadratic limb darkening coefficients as uniform priors, the package fits the Mandel & Agol (2002) transit model, considering the 29.5 minutes long cadence of K2 following Kipping (2010). As photometry data alone does not properly constrain the eccentricity, we assumed $e = 0$ in our fit, a reasonable assumption due to tidal circularization of orbits for close-in planets (Rodríguez et al. 2011).

The Mandel & Agol (2002) model considers a star limb darkening parametrized by a quadratic law with two coefficients, which were left as free parameters (with a uniform prior between 0 and 1) in the fitting process. For three candidates of our sample (EPIC 246909566 b, in the coolest star with $T_{\text{eff}} = 3057$ K, EPIC 248775938 b, in the hottest low-mass star with $T_{\text{eff}} = 4663$ K, and EPIC 248782482 b, in an intermediate T_{eff} star with $T_{\text{eff}} = 3852$ K), we also computed the planetary parameters fixing the quadratic limb-darkening coefficients to those tabulated in Claret (2018). The planetary parameters obtained are equal (within the uncertainties) than those obtained with the coefficients as free parameters in the `pyaneti` fit, so the coefficients were left as free parameters.

Appendix A (Figures A1, A2 and A3) shows the phase-folded transits and the best fit provided by `pyaneti`. The main derived parameters for our candidates are presented in Table A3.

To obtain the false positive probability (FPP) of our candidate list we used the `vespa` package⁹ (Morton 2015), which implements the procedure described in Morton (2012). The code computes the probabilities of planetary and non-planetary scenarios from very limited follow-up observations and Galaxy model simulations of stellar population. Using the TRILEGAL Galaxy model (Girardi et al. 2005), `vespa` considers different false positive scenarios caused by eclipsing binaries (EBs), background EBs (BEBs) and hierarchical triple systems (HEBs). `vespa` computes the stellar parameters from broadband photometry and parallaxes using `isochrones` and compares a large amount of simulated situations to the observed phase-folded light curve. Although

`vespa` considers the most frequent false positive scenarios involving eclipsing binaries, the package does not take into account other possible false positive scenarios as instrumental artifacts in the data or other astrophysical phenomena, such as star spots.

The package was run from the following inputs: coordinates, parallaxes from Gaia DR2, wide band BVHJKgr photometry, orbital period, transit phase-folded light curve, ratio R_p/R_* derived from `pyaneti`, maximum allowed depth of potential secondary eclipse (fixed with a value of 10^{-4}) and limits on the presence of nearby background stars derived from speckle and Pan-STARRS1 images.

The resulting FPPs for the candidates presented in this work and the multiplicity-corrected FPP₂ for those candidates belonging to a multi-planetary system are summarized in Table 3 and discussed in Section 5.

FPP computed by `vespa` could not be reliable if faint stars within the best aperture could be the sources of the signals. Also the full width at half-maximum (FWHM) of the point spread function (PSF) varies for Kepler between $3.1''$ and $7.5''$ ¹⁰, so targets outside the best aperture (but close to its edge) could also result in contamination. To discard this scenarios, we checked exhaustively all the targets, searching for nearby sources in Pan-STARRS1 and DSS2 images, Gaia DR2 and EPIC. The DSS2 images for the 22 stars are shown in Figure 7 along with the K2SFF apertures and Gaia DR2 nearby sources¹¹ (see the individual discussion in Section 5).

The relationship between the observed (δ') and true (δ) transit depth considering dilution from a secondary star within the best aperture and Δm magnitudes fainter than the brighter star is:

$$\delta' = \frac{\delta}{\gamma} = \frac{\delta}{1 + 10^{0.4 \Delta m}} \quad (2)$$

Assuming a conservative value of $\delta = 1$ (100 % dip in the faint secondary star), a value of $\delta' > \gamma^{-1}$ could not be originated in the secondary star, discarding the secondary star as the source of the signal. In all the cases with secondary stars within the best aperture or outside but at a distance $\lesssim 6''$ of its edge, we applied the criteria. If the secondary star is discarded as the origin of the signals (and the `vespa` FPP is $< 1\%$) the signal is validated. Otherwise the signal is considered as a candidate.

For each target, we also visually inspected the phase-folded light curves created using small and large apertures from the K2SFF photometric pipeline. In some cases, a nearby star a few pixels away from the target can be substantially excluded from the photometry using a small enough aperture. We find no apparent difference between the transit depths using a large and a small aperture except for EPIC 249391469 (see individual discussion in Section 5 for details).

In addition, for signals with FPP $< 1\%$, we only consider as validated planets those who fulfill the above criteria and also satisfies the condition $\text{SNR} > 10$, so signals with $6 < \text{SNR} < 10$ are considered as candidates.

¹⁰ According to Kepler documentation: <https://keplergo.arc.nasa.gov/DataAnalysisProducts.shtml>

¹¹ Figure 7 has been made using Astropy (Astropy Collaboration et al. 2013) and Astropyquery (Ginsburg et al. 2019).

⁸ <https://github.com/oscaribv/pyaneti>

⁹ <https://github.com/timothydmorton/VESPA>

ID	C	FPP	FPP ₂	Notes
EPIC 249384674 b	15	1.3×10^{-3}	7.2×10^{-5}	(2)
EPIC 249384674 c	15	4.2×10^{-4}	2.3×10^{-5}	(2)
EPIC 249391469 b	15	2.0×10^{-3}	–	(4, 5, 6)
EPIC 249557502 b	15	7.1×10^{-5}	–	(2)
EPIC 249826231 b	15	2.2×10^{-3}	–	(2)
EPIC 250001426 b	15	–	–	(2, 5)
EPIC 250099723 b	15	5.6×10^{-1}	–	(2)
EPIC 201663879 b	14	1.2×10^{-3}	3.0×10^{-5}	(1)
EPIC 201663879 c	14	5.0×10^{-1}	2.4×10^{-2}	(1)
EPIC 201796690 b	14	1.2×10^{-3}	–	(4)
EPIC 248480671 b	14	2.9×10^{-5}	–	(3)
EPIC 248558190 b	14	7.7×10^{-5}	–	(1)
EPIC 248616368 b	14	1.1×10^{-5}	–	(1)
EPIC 248639308 b	14	3.9×10^{-6}	–	(1)
EPIC 248775938 b	14	2.0×10^{-1}	–	(4)
EPIC 248782482 b	14	1.3×10^{-4}	–	(4, 5)
EPIC 246909566 b	13	5.2×10^{-2}	–	(4)
EPIC 245944983 b	12	–	–	(4)
EPIC 246074965 b	12	6.3×10^{-5}	–	(4)
EPIC 246163416 b	12	–	–	(1)
EPIC 246313886 b	12	6.0×10^{-3}	–	(4,7)
EPIC 246331347 b	12	2.0×10^{-2}	–	(4)
EPIC 246331418 b	12	9.5×10^{-4}	3.4×10^{-5}	(4, 5)
EPIC 246331418 c	12	2.2×10^{-3}	7.9×10^{-5}	(4, 5)
EPIC 246472939 b	12	1.0×10^{-3}	–	(4)

Table 3. False positive probabilities (FPP) from *vespa* and multiplicity-corrected probabilities (FPP₂) for all our candidates and validated planets except for EPIC 245944983 b (binary star), EPIC 250001426 b and EPIC 246163416 b (both with close stars detected in speckle images). Signals without computed FPP, with FPP > 1% or with FPP < 1% but not validated due to nearby companions within (or close to the edge of) the best aperture or due to not fulfilling the condition SNR > 10 are highlighted in red. (1): with limits on the presence of nearby background stars from speckle images from NESSI (WIYN telescope). (2): from speckle images from DSSI (GeminiS telescope). (3): from AO images at 2168 nm from NIRC2 (Keck telescope). (4): from Pan-STARRS1 images. (5): stars with FPP < 1% but not discarded contaminant sources detected within (or outside, but close to the edge of) the best aperture. (6): False positive. The signal comes from a nearby contaminant star. (7): Candidate status due to not fulfilling the imposed condition SNR > 10.

5 RESULTS & DISCUSSION

In Tables A1 and A2 we present respectively the photometry and *isochrones*-computed stellar parameters for the candidate host stars. Analysis of the candidate signals (see below) reveals that in fact one of them, detected in EPIC 201663913, is originated in the close early K-type star EPIC 201663879.

In Table A3 we present the computed candidate parameters for 21 of the 25 signals¹² detected in these 22 stars. 6 candidates belong to three multi-planetary candidate systems (EPIC 49384674, EPIC 201663879 and EPIC 246331418), with two candidates in each star.

¹² We have only tabulated the period, epoch and transit depth of the signal from the binary star EPIC 245944983, from EPIC 250001426 and EPIC 246163416, both with close stars detected in speckle images, and also from EPIC 249391469, whose signal comes from Gaia DR2 6239523158128298496 (see individual discussion).

We performed the false positive analysis with *vespa* for 22 signals. Due to photometric contamination, we do not computed FPP on the signal from the binary star EPIC 245944983, from EPIC 250001426 and from EPIC 246163416 (both with close stars detected in speckle images). The analysis concludes that 17 candidates have FPP < 1%, which is the common adopted threshold to statistically validate a planet (Rowe et al. 2014; Montet et al. 2015; Morton et al. 2016; Heller et al. 2019), but considering the nearby contaminant stars within the photometric aperture, 3 of these 17 candidates with FPP < 1% are considered as candidates instead of validated planets; 1 more signal is also considered a candidate for not satisfying the condition SNR > 10 and 1 signal is a false positive (see individual discussions in Section 5). 5 signals have 1% < FPP < 56%. Considering the false positive threshold as FPP > 90% (Montet et al. 2015), these 5 signals are also considered as planetary candidates, along with the remaining 3 signals from stars with close companions detected in speckle and Pan-STARRS1 images. We end up with 12 validated planets, 12 candidates and 1 false positive.

For the candidates in multi-planetary systems presented in this work we recalculated the false positive probabilities according to the low probability of multiple false positive signals (Lissauer et al. 2011). When two planet candidates are detected within the same aperture, these candidates have much lower FPPs than single candidates. Following Lissauer et al. (2012), for each candidate belonging to a multi-planetary system we computed the multiplicity-corrected false positive probability as FPP₂ = 1-P₂, where

$$P_2 \approx \frac{X_2 P_1}{X_2 P_1 + (1 - P_1)} \quad (3)$$

X₂ is the *multiplicity boost* for systems with two planet candidates and P₁ = 1-FPP, being FPP the false positive probability computed with *vespa* without considering the candidate multiplicity. The *multiplicity boost* can be estimated as the ratio between the fraction of analysed targets with planet candidates and the fraction of planet candidate hosts with more than one candidate. Lissauer et al. (2012) estimated X₂ ~ 25 for the prime Kepler mission but Sinukoff et al. (2016) argues that X₂ can not be assumed to be the same as that for K2, given the different Galactic backgrounds and pointing characteristics of the observations. The campaigns studied in this work have too few candidates to estimate X₂ properly (e.g. C14 and C15 have 0 published candidates), so we assumed the X₂ estimated for the adjoining well-studied campaigns C1, C2, C3 and C4. Using the catalog of Kruse et al. (2019), we computed X₂ ~ 28 for C3 (adjoining C12), X₂ ~ 26 for C4 (adjoining C13), X₂ ~ 40 for C1 (adjoining C14) and X₂ ~ 18 for C2 (adjoining C15). The FPPs for the validated planets and candidates (highlighted in red) are summarized in Table 3. For the planet candidates (1% < FPP < 90%), the main possible false positive scenarios are individually discussed below.

It is worth to mention that follow-up observations have revealed a false positive origin for several K2 validated planets. Shporer et al. (2017) identified three K2 validated Jupiter-sized planets as confirmed low-mass stellar secondaries. To explain the initial misclassification the authors state different possible causes as the indistinguishable ra-

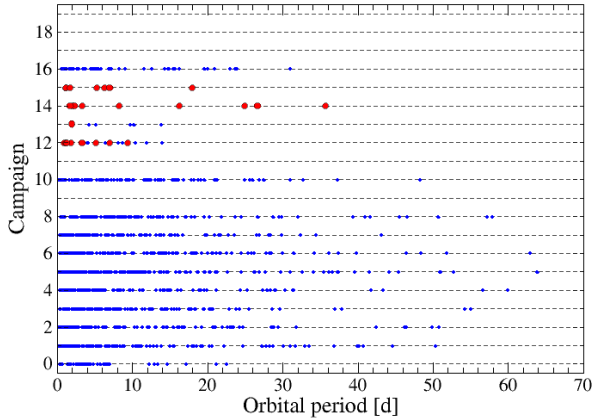


Figure 2. Orbital period distribution by Campaign of published K2 candidates and confirmed planets (blue) and the new candidates and validated planets presented in this work (red).

dius distribution of the smaller stars and gas giants planets, the difficulty in detecting a secondary eclipse in eccentric orbits and a poor characterization of the host star. Another source of misidentification can be the presence of an unnoticed background eclipsing binary within the photometric Kepler aperture, as we discuss below for our targets with background stars in the Pan-STARRS1 images and Gaia DR2. [Cabrera et al. \(2017\)](#) identified three K2 validated super-Earth-sized planets as background eclipsing binaries acquiring ground-based high-resolution images in which the binaries were left out of the photometric aperture. Although planet validation techniques are useful tools to get a quick approach to the goodness of planet candidates, there exist the possibility of misclassifications, so that detailed follow-up is necessary to confirm them.

In Figure 2 we plot the orbital period distribution of the new validated planets and candidates presented in this work and the previous published candidates and confirmed planets for each K2 campaign¹³. As mentioned in Section 2, only 8 candidates have been published in C12 and 5 in C13 by [Zink et al. \(2019\)](#), while C14 and C15 do not have published candidates.

Figure 3 plots the planet radii versus orbital periods for all the K2 previously published candidates and confirmed planets with $R < 25R_{\oplus}$, and the new validated planets and candidates presented in this work. 20 of them have orbital period $P_{\text{orb}} < 10 d$, 2 have $10 d < P_{\text{orb}} < 20 d$ and 3 have $P_{\text{orb}} > 20 d$. Regarding radii, 11 candidates and validated planets have $R < 2R_{\oplus}$, 9 have $2R_{\oplus} < R < 4R_{\oplus}$, and 1 has $R > 4R_{\oplus}$.

Figures 2 and 3 show that the number of candidates and planets decreases as the orbital period increases, especially after 40 days. Note that in this work we are only considering

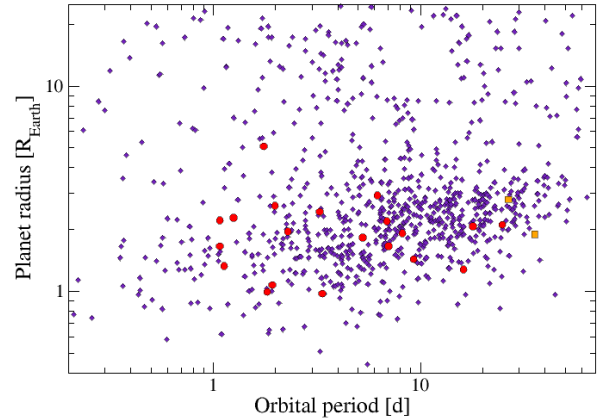


Figure 3. Planet radius versus orbital period for published K2 candidates and confirmed planets (violet) with $R_p < 25R_{\oplus}$ and candidates and validated planets from this work (red). Orange squares represent the validated planet b and candidate c in the early K-type star EPIC 201663879 ($T_{\text{eq}} = 5440 \text{ K}$), also from this work.

signals with at least three transits in the K2 light curve, which constrains periods to last less than 40 days. Figure 3 also shows a greater abundance of candidates with small radii. These trends are related to the short temporal span of the K2 observing windows and the intrinsic distribution of planets (66% have $P_{\text{orb}} < 10 d$ and 50% have $R < R_{\oplus}$).

Figure 4 shows the Kepler magnitude of the hosts stars versus the equilibrium temperature for all the confirmed planets, published K2 candidates and our validated and candidate planets. Two validated planets and two candidates are located in moderately bright stars ($k_p < 13$). EPIC 201663879 ($k_p = 11.93$) has two super-Earths (b, validated, $T_{\text{eq}} = 641 \text{ K}$, $R_p = 2.8 R_{\oplus}$, and c, candidate, $T_{\text{eq}} = 420 \text{ K}$, $R_p = 1.9 R_{\oplus}$). EPIC 248480671 ($k_p = 12.84$) hosts a validated super-Earth ($T_{\text{eq}} = 701 \text{ K}$, $R_p = 2.0 R_{\oplus}$), and EPIC 248782482 ($k_p = 12.59$) with a super-Earth candidate ($T_{\text{eq}} = 417 \text{ K}$, $R_p = 1.3 R_{\oplus}$). These are of special interest as they are well-suited for future radial velocity follow-up and atmospheric characterization.

Most of our validated planets and candidates receive large amounts of insolation (see Figure 5), computing $S_p > 5 S_{\oplus}$ for 18 of them. The habitable zone (HZ) is defined as the range of planet-star distances in which a planet could keep liquid water on its surface. As the presence of an atmosphere has a great impact on the surface temperature of a planet, several climate models in which different atmospheric constraints are considered provide different boundaries for the habitable zone.

[Kasting et al. \(1993\)](#) and [Kopparapu et al. \(2013\)](#) HZ boundaries exclude all our validated and candidate planets from the habitable zone. However, [Zsom et al. \(2013\)](#) state that the inner edge of the HZ for hot desert worlds, with low relative humidity and high albedos could be much closer to the star than previously thought. In particular, considering the optimistic proposed constrains of planets with 1% relative humidity and a terrestrial-like albedo ($A = 0.8$), 2

¹³ In all figures presented in this section we plot the data available at the NASA Exoplanet Archive (<https://exoplanetarchive.ipac.caltech.edu/>) for the previous published candidates and confirmed planets in all K2 campaigns.

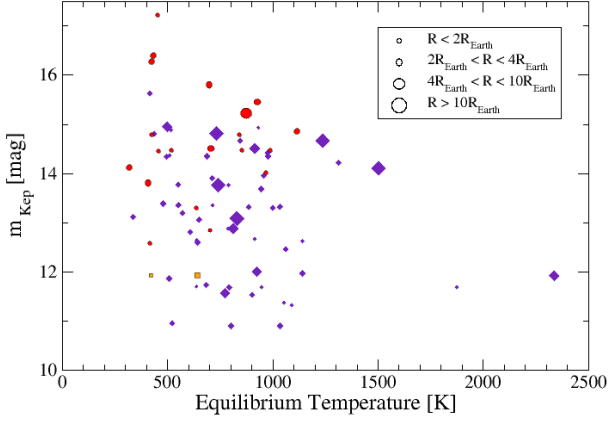


Figure 4. Kepler magnitude m_{Kep} of candidate hosts stars versus T_{eq} of candidate planets for published K2 (violet) and this work (red) candidates. Orange squares represent the validated planet b and candidate c in the early K-type star EPIC 201663879 ($T_{\text{eq}}=5440$ K), also from this work.

Candidate	C	Name	d_{in} [AU]	a [AU]
EPIC 250099723 b	15	–	0.1208	0.1417
EPIC 201663879 c	14	–	0.3038	0.3501
EPIC 248616368 b	14	K2-323 b	0.0922	0.1275
EPIC 248782482 b	14	–	0.0910	0.0999
EPIC 246074965 b	12	K2-325 b	0.0411	0.0419

Table 4. Validated planets and candidates within the habitable zone according to the optimistic Zsom model, considering 1% relative humidity and a terrestrial-like albedo ($A = 0.8$). The fourth column shows the distance to the host star of the inner edge of the habitable zone according to the Zsom model. The fifth column presents the computed orbital radius.

validated planets and 3 candidates presented in this work would be within the Zsom’s habitable zone, as detailed in the individual discussions (see Table 4).

Figure 6 plots the transit depth in logarithmic scale versus stellar magnitude in the Kepler band. Our validated planets and candidates follow the same upward trend that previously K2 published candidates and confirmed planets. This trend is related with the minimum signal-to-noise ratio $\text{SNR} = 6$ imposed in our transit search. In the figure we plot the transit depth detection limits for the typical orbital periods of the validated and candidate planets of our search (1.3, 3.7 and 17 days) with the selected SNR.

Of special interest are the warm super-Earth K2-323 b (validated, $T_{\text{eq}} = 318^{+24}_{-43}$ K, $S_p = 1.7 \pm 0.2 S_{\oplus}$, $R_p = 2.1 \pm 0.1 R_{\oplus}$), located in a $m_{\text{Kep}} = 14.13$ star, and the super-Earth EPIC 248782482 b (candidate, $T_{\text{eq}} = 417^{+58}_{-24}$ K, $S_p = 5.0 \pm 1.0 S_{\oplus}$, $R_p = 1.3 \pm 0.1 R_{\oplus}$) located in a moderately bright star ($m_{\text{Kep}} = 12.59$), thus being a good target for radial velocity follow-up and also for atmospheric characterization.

Next we will discuss the main features of each system, such as their statistical validation results, their physical parameters, and other individual aspects like habitability.

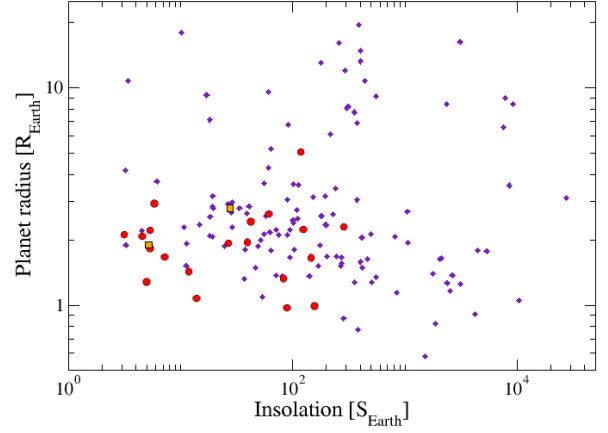


Figure 5. Planet radius versus insolation for published K2 candidates and confirmed planets (violet) with $R_p < 25R_{\oplus}$ and validated planets and candidates from this work (red). Orange squares represent the validated planet b and candidate c in the early K-type star EPIC 201663879 ($T_{\text{eq}} = 5440$ K), also from this work.

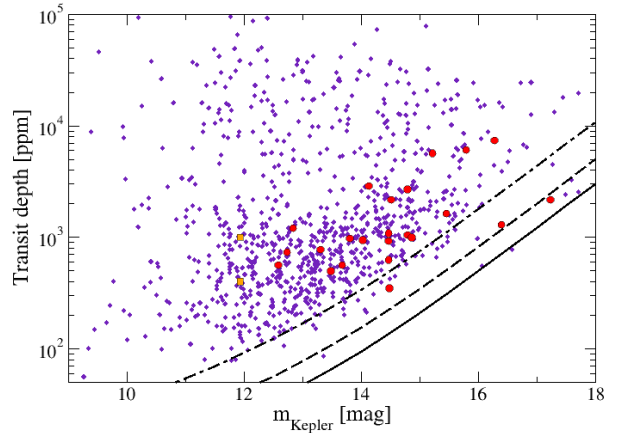


Figure 6. Transit depth versus m_{Kep} of candidate hosts stars for published K2 candidates and confirmed planets (violet) with transit depths $< 10\%$ and validated planets and candidates from this work (red). Orange squares represent the validated planet b and candidate c in the early K-type star EPIC 201663879 ($T_{\text{eq}} = 5440$ K), also from this work. The lines show the limits in transit depth detection for transiting planets with orbital period 1.3 days (solid line), 3.7 days (dashed line) and 17 days (dash-dotted line).

5.1 K2-316 (EPIC 249384674)

This target ($T_{\text{eff}} = 3436$ K, $R = 0.38 R_{\odot}$, $k_p = 14.79$) was observed in campaign 15 and shows two signals with periods 1.133 and 5.260 days. The speckle images (acquired with GeminiS) and contrast curves exclude companions with $\delta_{\text{mag}} < 4$ at $0.2''$. Also, analysis of Pan-STARRS1 archival images and Gaia DR2 discard the presence of possible nearby contaminant stars. In the analysis

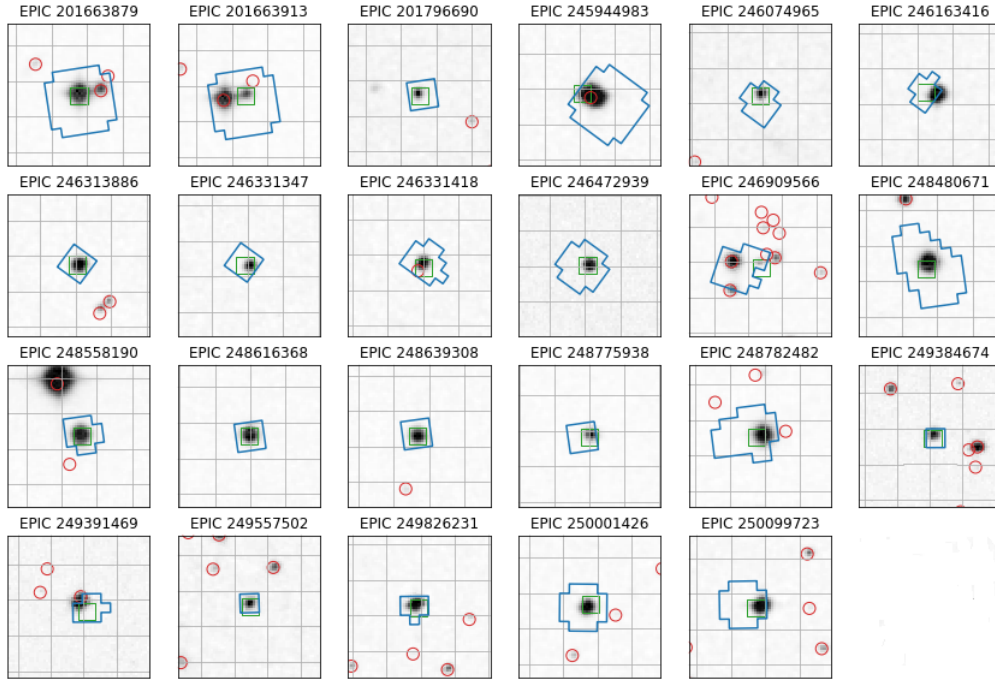


Figure 7. $1' \times 1'$ cut-out images from the DSS2 survey showing the target (green square) on the center and nearby Gaia sources (red circles). The photometric aperture (blue polygon) from the K2SFF pipeline is superposed. North is up and East is left.

with *vespa* we obtained independent false positive probabilities $FPP = 1.3 \times 10^{-3}$ for candidate b and $FPP = 4.2 \times 10^{-4}$ for candidate c. Both candidates separately are statistically validated. Anyway, considering that they are part of a multi-planetary system, we computed multiplicity-corrected false positive probabilities of $FPP_2 = 7.2 \times 10^{-5}$ for candidate b and $FPP_2 = 2.3 \times 10^{-5}$ for candidate c.

The non-detection of blended objects in speckle images, analysis of Pan-STARRS1 images and Gaia DR2, the FPPs $< 1\%$ from *vespa* and the low probability of multiple false positive signals makes this target a validated planetary system with two super-Earths ($R_b = 1.3 R_\oplus$ and $R_c = 1.8 R_\oplus$).

5.2 EPIC 249391469

This target ($T_{\text{eff}} = 3503 \text{ K}$, $R = 0.57 R_\odot$, $k_p = 14.03$, $\text{mag } G = 14.00$) was observed in campaign 15, showing a signal with a period of 1.075 days. Pan-STARRS1 image excludes stars with $\delta_{\text{mag}} < 4.5$ at 2.5 arc seconds and shows a faint source ($\text{mag } G = 19.42$) with an angular separation of $5.85''$ and position angle $PA = 172^\circ$, which is within the optimal aperture of the K2SFF (see Figure 7). As discussed in Section 4, the analysis of the phase-folded light curves created using small and large apertures from the K2SFF photometric pipeline shows a 2x increase in the transit depth when using a large aperture that includes the majority of the flux from the faint nearby star (see Figure 8). This indicates that the faint nearby star (Gaia DR2 6239523158128298496) is the actual source of the signal. The 9.5×10^{-4} transit depth implies a 14% dip, so the eclipsing binary scenario is the most likely. As a result, this signal is considered as a false positive.

5.3 K2-317 (EPIC 249557502)

This target ($T_{\text{eff}} = 3387 \text{ K}$, $R = 0.38 R_\odot$, $k_p = 16.40$) was observed in campaign 15 and shows a transit-like signal with a period of 6.220 days. The speckle image (acquired with GeminiS) excludes companions with $\delta_{\text{mag}} < 3$ at $0.1''$. The analysis of close stellar sources in Pan-STARRS1 images and Gaia DR2 discard photometric contamination. The *vespa* analysis results in $FPP = 7.1 \times 10^{-5}$, and it is thus a validated mini-Neptune with $R = 2.9 R_\oplus$.

The optimistic Zsom model places the inner edge of the habitable zone in this system at $d_{\text{in}} = 0.0546 \text{ AU}$ from the star (considering albedo = 0.8). Taking into account a derived semi-major axis $a = 0.0542 \text{ AU}$, this candidate might be orbiting close to the inner edge of the habitable zone.

5.4 K2-318 (EPIC 249826231)

This target ($T_{\text{eff}} = 3851 \text{ K}$, $R = 0.55 R_\odot$, $k_p = 14.47$) was observed in campaign 15 and exhibits a signal with a period of 7.010 days. The speckle image (acquired with GeminiS) excludes companions with $\delta_{\text{mag}} < 4$ at $0.2''$. Also the analysis of close stellar sources in Pan-STARRS-1 images and Gaia DR2 discard contamination. In the analysis with *vespa* we obtained $FPP = 2.2 \times 10^{-3}$, thus it is a validated planet. Our fit results in a super-Earth with $R = 1.7 R_\oplus$.

5.5 EPIC 250001426

This target was observed in campaign 15 and shows a signal with a period of 1.705 days. The speckle image (acquired with GeminiS) detected a secondary source at 0.23 arc seconds and $\Delta m \sim 0.4$. Following the criteria discussed in Sec-

tion 4, this candidate is not validated. As the photometry of both stars is mixed, we can not derive stellar nor planetary parameters.

5.6 EPIC 250099723

This target ($T_{\text{eff}} = 4176$ K, $R = 0.58 R_{\odot}$, $k_p = 13.80$) shows 5 transit events observed in campaign 15 with a period of 17.920 days. The speckle image (acquired with GeminiS) exclude companions with $\delta_{\text{mag}} < 4$ at $0.1''$. The Pan-STARRS1 and Gaia DR2 analysis of close stellar sources discard contamination. However, the analysis with *vespa* results in $\text{FPP} = 5.6 \times 10^{-1}$, so it remains a low-quality candidate. The most likely false positive scenario is the BEB, as its contribution to the total computed FPP is $\text{FPP}_{\text{BEB}} = 5.5 \times 10^{-1}$. Additional high precision photometric follow-up is needed to improve the signal, for which the best fit is considerably flat-bottomed with the 5 transits observed by K2.

The signal is modelled by a candidate super-Earth with $R = 2.1 R_{\oplus}$. The inner edge of the habitable zone in the optimistic Zsom model is located at $d_{\text{in}} = 0.1208$ AU (adopting $A = 0.8$ albedo). Our estimated orbital radius for this candidate is $a = 0.1417$ AU, so it would be in or traversing the habitable zone of the star.

5.7 K2-319 (EPIC 201663879) / EPIC 201663913

In campaign 14, 3 transit events with a period of 26.718 days were detected in EPIC 201663913 ($T_{\text{eff}} = 3874$ K, $R = 0.68 R_{\odot}$, $k_p = 14.45$). The image from Pan-STARRS1 shows a brighter star (K2-319, $k_p = 11.93$) at an angular distance of $10''$ and $\text{PA} = 102.4^{\circ}$. Stellar parameters for K2-319 derived from *isochrones* are $T_{\text{eff}} = 5440$ K, $R = 0.90 R_{\odot}$, $\log g = 4.5$. The 26.718-day signal is also present at K2-319.

Suspecting contamination, we searched for transit signals in EPIC 201663913 with smaller apertures in its K2SFF corrected light curve, finding that the signal disappears and confirming that it comes from K2-319. Posterior light curve analysis of K2-319 showed, in addition to the initial signal, another signal with a period of 35.621 days and three transits, and also two more transit-like features that suggest the presence of more candidates.

The speckle image of K2-319 acquired at the 3.5 m WIYN telescope rules out the presence of blended targets with $\delta_{\text{mag}} < 4$ at $0.5''$. Also, analysis of close stars with Pan-STARRS1 images and Gaia DR2 discard possible contaminant sources (except EPIC 201663913, but as discussed, this M dwarf is not the source of the signals). We performed a statistical validation of this signal with *vespa*, obtaining $\text{FPP} = 1.2 \times 10^{-3}$ for candidate b, and $\text{FPP} = 5.0 \times 10^{-1}$ for candidate c. Considering that the candidates are in a multi-planetary system, the multiplicity-corrected false positive probabilities are $\text{FPP}_2 = 3.0 \times 10^{-5}$ for candidate b and $\text{FPP}_2 = 2.4 \times 10^{-2}$ for candidate c. Candidate b is considered to be statistically validated. Since the signal c originates from a multi-signal system, the most plausible scenario is a planetary origin. Even so, the analysis with *vespa* yields a $\text{FPP} > 1\%$ so it remains in the candidate status, being the EB the main possible false positive scenario.

Assuming the stellar parameters indicated above for K2-319, the validated planet b is modeled as a mini-Neptune with $R = 2.8 R_{\oplus}$ and the candidate c as a super-Earth with $R = 1.9 R_{\oplus}$.

The optimistic Zsom model for habitable zones indicates for this system a inner edge situated at $d_{\text{in}} = 0.3038$ AU from the star (considering albedo = 0.8). Taking into account a derived semi-major axis $a = 0.3501$ AU for the candidate c, this might be in the habitable zone.

With $k_p = 11.93$, this system is a good target for radial velocity follow-up, in order to characterize the masses and detect the presence of more planets, and for their atmospheric characterization.

5.8 K2-320 (EPIC 201796690)

This target ($T_{\text{eff}} = 3157$ K, $R = 0.30 R_{\odot}$, $k_p = 15.80$) was observed in campaign 14 and exhibits a transit-like signal with a period of 1.995 days. The Pan-STARRS1 image shows no blended sources, excluding stars with $\delta_{\text{mag}} < 5.1$ at $2.5''$. Also, analysis of Pan-STARRS1 images and Gaia DR2 discard possible nearby contaminant sources. Our fit points to a super-Earth candidate with $R = 2.6 R_{\oplus}$. The *vespa* analysis computed $\text{FPP} = 1.2 \times 10^{-3}$, and it is thus a statistically validated planet.

5.9 K2-321 (EPIC 248480671)

This target ($T_{\text{eff}} = 3855$ K, $R = 0.58 R_{\odot}$, $k_p = 12.84$) was observed in campaign 14 and shows a transit-like signal with a period of 2.298 days. The AO image acquired at Keck discard the presence of close stars. In particular, the observations showed no additional stellar companions to within a resolution $\sim 0.06''$ FWHM and out to $8''$. Also, inspection of Pan-STARRS1 images and Gaia DR2 discard possible nearby contaminant sources. The analysis performed with *vespa* results in $\text{FPP} = 2.9 \times 10^{-5}$, making this a statistically validated planet, whose fit corresponds to a $2.0 R_{\oplus}$ super-Earth.

5.10 K2-322 (EPIC 248558190)

This star ($T_{\text{eff}} = 4141$ K, $R = 0.60 R_{\odot}$, $k_p = 13.31$) was observed in campaign 14 and shows a signal with an 8.205-day period. The speckle image (acquired at 3.5 m WIYN telescope) exclude blended objects with $\delta_{\text{mag}} < 4$ at $0.2''$ and $\delta_{\text{mag}} < 5$ at $0.5''$. Analysis of Pan-STARRS1 images and Gaia DR2 shows a faint source (mag G = 20.22) at $12.6''$, outside the optimal aperture (of radius $\sim 8''$), but very close to the edge. Assuming depth = 0.8 ppt, we modelled the flux distribution, resulting in a partial flux of $\sim 12\%$ within the aperture, ruling out this faint star as the source of the signal. The analysis with *vespa* results in $\text{FPP} = 7.7 \times 10^{-5}$, thus making it a validated planet. The fit results in a super-Earth with $1.9 R_{\oplus}$. Also a single transit event is detected in epoch 3105.28 BKJD showing a ~ 2 ppt transit depth. A specific photometric or RV follow-up is necessary to confirm this signal, which could be associated with a $\sim 3R_{\oplus}$ mini-Neptune (see Figure 1).

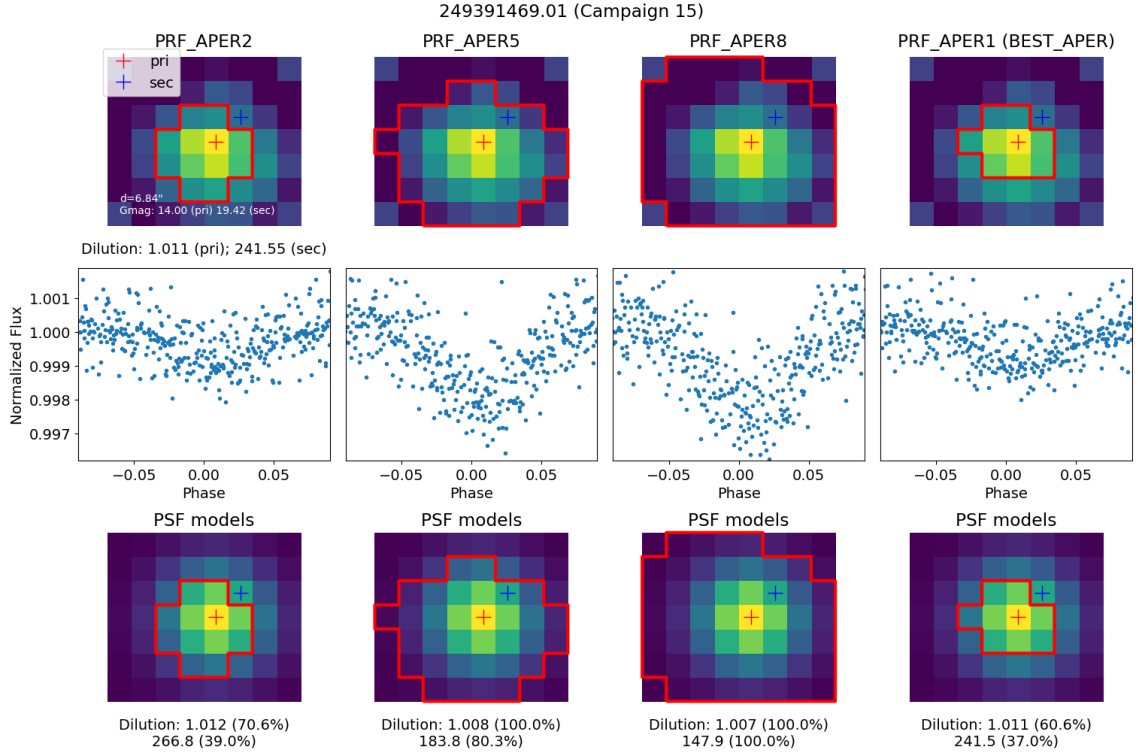


Figure 8. Phase-folded light curves created using small and large apertures from the K2SFF photometric pipeline for EPIC 249391469. The red crosses corresponds to the primary star and the blue crosses to the faint nearby star. The central plots shows larger apertures (PRF_APER5 and PRF_APER8), which include the majority of the flux from the faint nearby star. For these apertures, the relative flux dimming is two times greater than in a situation in which the secondary source is left out of the aperture (PRF_APER2 and PRF_APER1). This result indicates that the faint nearby star (Gaia DR2 6239523158128298496) is the actual source of the signal. The transit depth implies a 14% dip, so the eclipsing binary scenario is the most likely, making this signal a false positive.

5.11 K2-323 (EPIC 248616368)

This star ($T_{\text{eff}} = 3710$ K, $R = 0.55 R_{\odot}$ & $k_p = 14.13$) was observed in campaign 14 and shows 3 transit events with a period of 24.930 days. The speckle image (acquired at the 3.5 m WIYN telescope) excludes close companions with $\delta_{\text{mag}} < 3$ at $0.2''$ and $\delta_{\text{mag}} < 4$ at $0.5''$. The analysis of nearby stars with Pan-STARRS1 images and Gaia DR2 discard contaminant sources. The *vespa* analysis results in $\text{FPP} = 1.1 \times 10^{-5}$, thus making it a validated planet whose fit models a $2.1 R_{\oplus}$ super-Earth.

This validated planet is moderately warm, with $T_{\text{eq}} = 318^{+24}_{-43}$ K and $S_p = 1.7 \pm 0.2 S_{\oplus}$. The optimistic Zsom model for habitable zones indicates for this system an inner edge situated at $d_{\text{in}} = 0.0922$ AU from the star (considering albedo = 0.8). Taking into account a derived semi-major axis $a = 0.1275$ AU, this super-Earth might be in the habitable zone.

5.12 K2-324 (EPIC 248639308)

This target ($T_{\text{eff}} = 3752$ K, $R = 0.51 R_{\odot}$, $k_p = 14.51$) was observed in campaign 14 and exhibits a signal with a period of 3.262 days. The speckle image (acquired at the 3.5 m WIYN telescope) discards blended stars with $\delta_{\text{mag}} < 3.5$ at $0.2''$ and $\delta_{\text{mag}} < 5$ at $0.5''$. The analysis of Pan-STARRS1 images and Gaia DR2 discard nearby contaminant stars. *vespa* statistical analysis concluded with $\text{FPP} = 3.9 \times 10^{-6}$,

thus making it a validated planet whose fit corresponds to a super-Earth with $2.4 R_{\oplus}$.

5.13 EPIC 248775938

This target ($T_{\text{eff}} = 4663$ K, $R = 0.61 R_{\odot}$, $k_p = 15.22$) was observed in campaign 14 and according to its *isochrones* fit, it has the highest temperature of the characterized stars in this work, with the exception of the early K-type star EPIC 201663879. It shows a transit-like signal with a period of 1.743 days. No close companions or blended stars are present in the images from Pan-STARRS1, excluding stars with $\delta_{\text{mag}} < 4.7$ at $2.5''$. Also, analysis of pan-STARRS1 images and Gaia DR2 shows no nearby sources, discarding contamination. Our fit points to a $5.1 R_{\oplus}$ Neptune-like candidate, being the candidate with the largest radius presented in this work. The phase folded light curve is quite v-shaped, with the *vespa* analysis resulting in a computed $\text{FPP} = 2.0 \times 10^{-1}$. The most likely false positive scenario is the EB, as its contribution to the total computed FPP is $\text{FPP}_{\text{EB}} = 1.9 \times 10^{-1}$.

5.14 EPIC 248782482

This star ($T_{\text{eff}} = 3852$ K, $R = 0.50 R_{\odot}$, $k_p = 12.59$) was observed in campaign 14. It is the brightest of all the low-mass candidate hosts in our list (with the exception of the

early K-type EPIC 201663879, $k_p = 11.93$) and shows 5 transit events with a period of 16.222 days. Pan-STARRS1 image shows no evidence of close or blended sources, excluding stars with $\delta_{mag} < 4.3$ at $2.5''$. However, in Pan-STARRS1 images and Gaia DR2 we find a mag G = 19.77 star within the optimal aperture which we can't rule out as the source of the signal, so although *vespa* analysis computed $FPP = 1.3 \times 10^{-4}$, we can not validate this candidate.

Our fit points to a $1.3 R_{\oplus}$ super-Earth with $T_{eq} = 417_{-24}^{+58}$ K and $S_p = 5.0 \pm 0.1 S_{\oplus}$. The optimistic Zsom model for habitable zones indicates for this system an inner edge situated at $d_{in} = 0.0910$ AU from the star (considering albedo = 0.8). Taking into account a derived semi-major axis $a = 0.0999$ AU, this super-Earth candidate might be in the habitable zone.

The moderately-high brightness of the star makes this candidate an interesting target for radial velocity follow up that could make it possible to confirm the planet, measure its mass, study the possible presence of more planets in the system and their atmospheric characterization.

5.15 EPIC 246909566

This target ($T_{eff} = 3067$ K, $R = 0.24 R_{\odot}$, $k_p = 17.23$) was observed in campaign 13 and it is the coolest and faintest star in our candidate hosts list, showing a 1.925-day periodic signal. It is located in a moderately-crowded field with several nearby faint stars at angular distances $> 6''$. No blended sources are present in Pan-STARRS1 image, excluding stars with $\delta_{mag} < 4.2$ at $2.5''$. However, analysis of Pan-STARRS1 images and Gaia DR2 shows two stars within the optimal aperture (mag G = 13.81 at $12''$ and mag G = 20.51 at $4.8''$) which we can not rule out as the sources of the signal. Furthermore, the *vespa* analysis computes $FPP = 5.2 \times 10^{-2}$. The most likely false positive scenario is the BEB with a contribution to the total FPP of $FPP_{BEB} = 4.8 \times 10^{-2}$. The fit suggests an Earth-size candidate with $1.1 R_{\oplus}$.

5.16 EPIC 245944983

This target was observed in campaign 12 and its light curve shows a signal with a period of 5.138 days. This is a binary system; according to Gaia DR2, both stars are situated at the same distance (140 pc) and exhibit almost identical proper motions ($\mu_{\alpha} \sim 109$ mas, $\mu_{\delta} \sim 25$ mas). The angular separation between the components is $\sim 4''$.

The K2 detector has an image scale of $3.98''$ per pixel, so the photometry of both sources is blended in the light curve. This signal needs a specific photometric follow-up with a resolution of $\sim 1''$ to distinguish in which component the signal originates and to model the candidate parameters properly.

5.17 K2-325 (EPIC 246074965)

This star ($T_{eff} = 3287$ K, $R = 0.30 R_{\odot}$, $k_p = 16.28$) was observed in campaign 12 and shows a transit-like signal with a period of 6.930 days. The image from Pan-STARRS1 shows no evidence of close or blended companions, excluding stars with $\delta_{mag} < 4.9$ at $2.5''$. Also the Pan-STARRS1 images and Gaia DR2 analysis discard nearby contaminant stars. Our fit models a super-Earth with $R = 2.2 R_{\oplus}$ and *vespa* analysis

computed a $FPP = 6.3 \times 10^{-5}$, thus making it a statistically validated planet.

The optimistic Zsom model for habitable zones indicates for this system an inner edge situated at $d_{in} = 0.0411$ AU from the star (considering albedo = 0.8). Taking into account a derived semi-major axis $a = 0.0419$ AU, this super-Earth might be in the habitable zone.

5.18 EPIC 246163416

This target was observed in campaign 12 and exhibits a signal with a period of 0.877 days. The speckle image (acquired with NESSI instrument at WIYN-3.5m) detected a secondary source at $0.66''$ and $\Delta m = 1.39$, so we can not distinguish which star is the source of the signal, nor derive the stellar or planetary parameters.

5.19 EPIC 246313886

This target ($T_{eff} = 3949$ K, $R = 0.50 R_{\odot}$, $k_p = 14.48$) was observed in campaign 12 and shows a periodic signal with 1.827-day period. Pan-STARRS1 image shows no close or blended stars, excluding stars with $\delta_{mag} < 4.9$ at $2.5''$. Also analysis of Pan-STARRS1 images and Gaia DR2, discards contamination from nearby stars. We fit the signal as an Earth-size candidate with $1.0 R_{\oplus}$ and the *vespa* analysis resulted in $FPP = 6.0 \times 10^{-3}$. However the computed signal-to-noise ratio does not meet the condition $SNR > 10$, so we consider this signal as a candidate.

5.20 EPIC 246331347

This target ($T_{eff} = 3408$ K, $R = 0.52 R_{\odot}$, $k_p = 15.46$) was observed in campaign 12 and shows a signal with a period of 1.082 days. The Pan-STARRS1 image does not show close or blended stars, excluding stars with $\delta_{mag} < 5.9$ at $2.5''$. Analysis of Pan-STARRS1 images and Gaia DR2 discard contamination from nearby stars. However, the *vespa* analysis computed $FPP = 2.0 \times 10^{-2}$ with all the contribution to the FPP from the BEB scenario. Our fit points to a super-Earth candidate with $2.2 R_{\oplus}$.

5.21 EPIC 246331418

This target ($T_{eff} = 4408$ K, $R = 0.43 R_{\odot}$, $k_p = 14.47$) was observed in campaign 12 and shows two transit-like signals with periods 3.350 and 9.320 days. However, the Pan-STARRS1 image shows a faint star at an angular distance of $3''$ (PA = 125.8°), smaller than the pixel scale of K2 and well within the optimal aperture. According to Gaia DR2, both stars lie at the same distance ($\pi = 6.34 \pm 0.04''$ and $\pi = 5.54 \pm 1.20''$ for the primary and secondary respectively) and present the same proper motions ($\mu_{\alpha} = -19.89 \pm 0.08$ mas \cdot yr $^{-1}$, $\mu_{\delta} = -53.64 \pm 0.06$ mas \cdot yr $^{-1}$ for the primary and $\mu_{\alpha} = -20.25 \pm 2.51$ mas \cdot yr $^{-1}$, $\mu_{\delta} = -53.89 \pm 2.61$ mas \cdot yr $^{-1}$ for the secondary), making it a binary system.

With the distance and the G magnitude from Gaia DR2, we estimated an absolute magnitude for the secondary of $M_G \sim 14.3$. With this M_G , we estimated from the [Pecaut & Mamajek \(2013\)](#) tabulated parameters a M5V spectral

type for the secondary, with $T \sim 3030$ K, $R \sim 0.20 R_{\odot}$ and $M \sim 0.15 M_{\odot}$.

A planetary origin for the signals, both in the same star, is the most likely scenario as the other combinations involving transiting planets and eclipsing binaries have extremely low probabilities. However, it is not possible to distinguish which of both stars is the source of the signals, so they are considered as candidates. Even so, taking into account the 6.3×10^{-4} and 1.0×10^{-3} mag transit depths for candidates b and c, if both signals were originated in the secondary, it would imply a 9% and 16% decreases in the secondary flux for candidates b and c respectively. As discussed above, adopting $R \sim 0.20 R_{\odot}$ for the star, the radii of the candidates would be estimated at $\sim 0.6 R_J$ (b) and $\sim 0.8 R_J$ (c). Finding two gas giants on a low mass star is extremely unlikely as only a few Jupiter-mass exoplanets have been found orbiting low mass stars (Delfosse et al. 1998; Marcy et al. 1998; Morales et al. 2019). All these considerations make the primary as the most likely host for the candidates.

Assuming the primary as the host star, our fit results in candidates with radii 1.0 and $1.4 R_{\oplus}$. The computed false positive probabilities from *vespa* are $FPP = 9.5 \times 10^{-4}$ (b) and $FPP = 2.2 \times 10^{-3}$ (c), and the multiplicity-corrected false positive probabilities are $FPP_2 = 3.4 \times 10^{-5}$ (b) and $FPP_2 = 7.9 \times 10^{-5}$ (c), anyway these signals are not validated, as discussed before.

5.22 K2-326 (EPIC 246472939)

This target ($T_{\text{eff}} = 3924$ K, $R = 0.69 R_{\odot}$, $k_p = 14.87$) was observed in campaign 12 and shows a candidate signal with a period of 1.256 days. Pan-STARRS1 image shows no close or blended stars, excluding stars with $\delta_{\text{mag}} < 5.1$ at $2.5''$. Also analysis of Pan-STARRS1 images and Gaia DR2 discard nearby contaminant stars. We fit this signal as a $2.3 R_{\oplus}$ super-Earth and the *vespa* analysis computed $FPP = 1.0 \times 10^{-3}$, thus it is a validated planet.

6 CONCLUSIONS

Our analysis of the photometry of 20038 cool stars from campaigns 12, 13, 14 and 15 of the K2 mission resulted in a catalogue of 12 new statistically validated planets, 12 planetary candidates and 1 false positive, distributed among 22 stars.

We computed the stellar parameters for 19 stars from their colours and accurate distances from Gaia. We derived the candidate parameters for all the systems (except for the binary EPIC 245944983, EPIC 250001426 and EPIC 246163416, both with close stars detected in speckle images, and the false positive EPIC 249391469) and also presented their phase-folded light curves along with their best fit.

Six of these signals belong to three multi-planetary systems, with two signals in each system (EPIC 249384674, EPIC 201663879 and EPIC 246331418).

Both validated planets and candidates from this work cover a wide range of orbital periods, between 0.877 d and 35.621 d, but they mostly have short periods, with a median value of 3.350 d.

2 validated planets and 2 candidates are located in

moderately bright stars ($m_{\text{kep}} < 13$), making these systems good targets for radial velocity follow-up and atmospheric characterization. 2 validated planets and 3 candidates have estimated orbital radius within the limits of the habitable zone according to the optimistic Zsom model. Of special interest are the warm super-Earth K2-323 b (validated, $T_{\text{eq}} = 318^{+24}_{-43}$ K, $S_p = 1.7 \pm 0.2 S_{\oplus}$, $R_p = 2.1 \pm 0.1 R_{\oplus}$), located in a $m_{\text{kep}} = 14.13$ star, and the super-Earth EPIC 248782482 b (candidate, $T_{\text{eq}} = 417^{+58}_{-24}$ K, $S_p = 5.0 \pm 1.0 S_{\oplus}$, $R_p = 1.28 \pm 0.1 R_{\oplus}$) located in a moderately bright star ($m_{\text{kep}} = 12.59$), thus being a good targets for radial velocity follow-up and also for atmospheric characterization with transmission techniques with high resolution spectrographs such as ESPRESSO at VLT (Pepe et al. 2014; González Hernández et al. 2018).

Future radial velocity and photometric follow-up are necessary in order to confirm the candidates presented in this work. Meanwhile, detailed analysis of the light curves acquired by missions such as the Kepler Space Telescope, with the aim of detecting undiscovered candidate signals, will continue to provide valuable information for our understanding of planetary systems.

ACKNOWLEDGEMENTS

ACG, EDA, SLSG, CGG, FGR and JCJ would like to acknowledge Spanish ministry project AYA2017-89121-Psystems. LB acknowledges financial support from the PGC 2018 project PGC2018-101948-B-I00 (MICINN, FEDER).

This paper includes data collected by the Kepler mission and obtained from the MAST data archive at the Space Telescope Science Institute (STScI). Funding for the Kepler mission is provided by the NASA Science Mission Directorate. STScI is operated by the Association of Universities for Research in Astronomy, Inc., under NASA contract NAS 5-26555.

The Pan-STARRS1 Surveys (PS1) and the PS1 public science archive have been made possible through contributions by the Institute for Astronomy, the University of Hawaii, the Pan-STARRS Project Office, the Max-Planck Society and its participating institutes, the Max Planck Institute for Astronomy, Heidelberg and the Max Planck Institute for Extraterrestrial Physics, Garching, The Johns Hopkins University, Durham University, the University of Edinburgh, the Queen's University Belfast, the Harvard-Smithsonian Center for Astrophysics, the Las Cumbres Observatory Global Telescope Network Incorporated, the National Central University of Taiwan, the Space Telescope Science Institute, the National Aeronautics and Space Administration under Grant No. NNX08AR22G issued through the Planetary Science Division of the NASA Science Mission Directorate, the National Science Foundation Grant No. AST-1238877, the University of Maryland, Eotvos Lorand University (ELTE), the Los Alamos National Laboratory, and the Gordon and Betty Moore Foundation.

This research has made use of the Exoplanet Follow-up Observation Program website, which is operated by the California Institute of Technology, under contract with the National Aeronautics and Space Administration under the Exoplanet Exploration Program.

This research has made use of the NASA Exoplanet

Archive, which is operated by the California Institute of Technology, under contract with the National Aeronautics and Space Administration under the Exoplanet Exploration Program.

This work has made use of data from the European Space Agency (ESA) mission *Gaia* (<https://www.cosmos.esa.int/gaia>), processed by the *Gaia* Data Processing and Analysis Consortium (DPAC, <https://www.cosmos.esa.int/web/gaia/dpac/consortium>). Funding for the DPAC has been provided by national institutions, in particular the institutions participating in the *Gaia* Multilateral Agreement.

The Digitized Sky Surveys were produced at the Space Telescope Science Institute under U.S. Government grant NAG W-2166. The images of these surveys are based on photographic data obtained using the Oschin Schmidt Telescope on Palomar Mountain and the UK Schmidt Telescope. The plates were processed into the present compressed digital form with the permission of these institutions.

Some of the observations in the paper made use of the NN-EXPLORE Exoplanet and Stellar Speckle Imager (NESSI). NESSI was funded by the NASA Exoplanet Exploration Program and the NASA Ames Research Center. NESSI was built at the Ames Research Center by Steve B. Howell, Nic Scott, Elliott P. Horch, and Emmett Quigley.

We thank Joaquin González-Nuevo for useful discussions.

REFERENCES

- Aguado D. S., et al., 2019, *ApJS*, 240, 23
- Ahn C. P., et al., 2012, *ApJS*, 203, 21
- Asplund M., Grevesse N., Sauval A. J., Scott P., 2009, *ARA&A*, 47, 481
- Astropy Collaboration et al., 2013, *aap*, 558, A33
- Barragán O., Gandolfi D., Antoniciello G., 2019, *MNRAS*, 482, 1017
- Batalha N. M., et al., 2013, *ApJS*, 204, 24
- Borucki W. J., et al., 2010, *Science*, 327, 977
- Borucki W. J., et al., 2011, *ApJ*, 736, 19
- Burke C. J., et al., 2014, *ApJS*, 210, 19
- Cabrera J., et al., 2017, *A&A*, 606, A75
- Chambers K. C., et al., 2016, arXiv e-prints, p. arXiv:1612.05560
- Charbonneau D., Brown T. M., Noyes R. W., Gilliland R. L., 2002, *ApJ*, 568, 377
- Choi J., Dotter A., Conroy C., Cantiello M., Paxton B., Johnson B. D., 2016, *ApJ*, 823, 102
- Claret A., 2018, *A&A*, 618, A20
- Crossfield I. J. M., et al., 2016, *ApJS*, 226, 7
- David T. J., et al., 2018, *AJ*, 155, 222
- Delfosse X., Forveille T., Mayor M., Perrier C., Naef D., Queloz D., 1998, *A&A*, 338, L67
- Díez Alonso E., et al., 2018a, *MNRAS*, 476, L50
- Díez Alonso E., et al., 2018b, *MNRAS*, 480, L1
- Díez Alonso E., et al., 2019, *MNRAS*, 489, 5928
- Dotter A., 2016, *ApJS*, 222, 8
- Dressing C. D., Charbonneau D., 2013, *ApJ*, 767, 95
- Dressing C. D., Charbonneau D., 2015, *ApJ*, 807, 45
- Dressing C. D., et al., 2019, *AJ*, 158, 87
- Flewelling H., 2018, in American Astronomical Society Meeting Abstracts #231. p. 436.01
- Furlan E., et al., 2017, *AJ*, 153, 71
- Gaia Collaboration et al., 2018, *A&A*, 616, A1
- Gillon M., et al., 2017, *Nature*, 542, 456
- Ginsburg A., et al., 2019, *AJ*, 157, 98
- Girardi L., Groenewegen M. A. T., Hatziminaoglou E., da Costa L., 2005, *A&A*, 436, 895
- González Hernández J. I., Pepe F., Molaro P., Santos N. C., 2018, *ESPRESSO on VLT: An Instrument for Exoplanet Research*. p. 157, doi:10.1007/978-3-319-55333-7_157
- Hardegree-Ullman K. K., Zink J. K., Christiansen J. L., Dressing C. D., Ciardi D. R., Schlieder J. E., 2020, *ApJS*, 247, 28
- Hartman J. D., Bakos G. Á., 2016, *Astronomy and Computing*, 17, 1
- Heller R., Hippke M., Rodenbeck K., 2019, *A&A*, 627, A66
- Henry T. J., Jao W.-C., Subasavage J. P., Beaulieu T. D., Ianna P. A., Costa E., Méndez R. A., 2006, *AJ*, 132, 2360
- Horch E. P., Veillette D. R., Baena Gallé R., Shah S. C., O’Rielly G. V., van Altena W. F., 2009, *AJ*, 137, 5057
- Horch E. P., Gomez S. C., Sherry W. H., Howell S. B., Ciardi D. R., Anderson L. M., van Altena W. F., 2011, *AJ*, 141, 45
- Howard A. W., et al., 2012, *ApJS*, 201, 15
- Howell S. B., Everett M. E., Sherry W., Horch E., Ciardi D. R., 2011, *AJ*, 142, 19
- Howell S. B., et al., 2014, *PASP*, 126, 398
- Huber D., et al., 2016, *ApJS*, 224, 2
- Kasting J. F., Whitmire D. P., Reynolds R. T., 1993, *Icarus*, 101, 108
- Kipping D. M., 2010, *MNRAS*, 408, 1758
- Kopparapu R. K., et al., 2013, *ApJ*, 765, 131
- Kovács G., Zucker S., Mazeh T., 2016, *BLS: Box-fitting Least Squares, Astrophysics Source Code Library (ascl:1607.008)*
- Kruse E., Agol E., Luger R., Foreman-Mackey D., 2019, *ApJS*, 244, 11
- Lissauer J. J., et al., 2011, *ApJS*, 197, 8
- Lissauer J. J., et al., 2012, *ApJ*, 750, 112
- Livingston J. H., et al., 2018a, *AJ*, 156, 78
- Livingston J. H., et al., 2018b, *AJ*, 156, 277
- Lohmann A. W., Weigelt G., Wirtzner B., 1983, *Appl. Opt.*, 22, 4028
- Malo L., Doyon R., Lafrenière D., Artigau É., Gagné J., Baron F., Riedel A., 2013, *ApJ*, 762, 88
- Mandel K., Agol E., 2002, *ApJ*, 580, L171
- Marcy G. W., Butler R. P., Vogt S. S., Fischer D., Lissauer J. J., 1998, *ApJ*, 505, L147
- Marigo P., Girardi L., Bressan A., Groenewegen M. A. T., Silva L., Granato G. L., 2008, *A&A*, 482, 883
- Meng J., Aitken G. J. M., Hege E. K., Morgan J. S., 1990, *Journal of the Optical Society of America A*, 7, 1243
- Montet B. T., et al., 2015, *ApJ*, 809, 25
- Morales J. C., et al., 2019, *Science*, 365, 1441
- Morton T. D., 2012, *ApJ*, 761, 6
- Morton T. D., 2015, *isochrones: Stellar model grid package, Astrophysics Source Code Library (ascl:1503.010)*
- Morton T. D., Bryson S. T., Coughlin J. L., Rowe J. F., Ravichandran G., Petigura E. A., Haas M. R., Batalha N. M., 2016, *ApJ*, 822, 86
- Mulders G. D., Pascucci I., Apai D., 2015a, *ApJ*, 798, 112
- Mulders G. D., Pascucci I., Apai D., 2015b, *ApJ*, 814, 130
- Paxton B., Bildsten L., Dotter A., Herwig F., Lesaffre P., Timmes F., 2011, *ApJS*, 192, 3
- Paxton B., et al., 2015, *ApJS*, 220, 15
- Pecaut M. J., Mamajek E. E., 2013, *The Astrophysical Journal Supplement Series*, 208, 9
- Pepe F., et al., 2014, *Astronomische Nachrichten*, 335, 8
- Pope B. J. S., Parviainen H., Aigrain S., 2016, *MNRAS*, 461, 3399
- Ricker G. R., et al., 2014, *Transiting Exoplanet Survey Satellite (TESS)*. p. 914320, doi:10.1117/12.2063489
- Rodríguez D., 2016, *dr-rodriguez/Kinematics-App: Stellar Kinematics v1.0*, doi:10.5281/zenodo.192159, <https://doi.org/10.5281/zenodo.192159>

- Rodríguez A., Ferraz-Mello S., Michtchenko T. A., Beaugé C., Miloni O., 2011, *MNRAS*, 415, 2349
- Rowe J. F., et al., 2014, *ApJ*, 784, 45
- Schmitt A. R., Hartman J. D., Kipping D. M., 2019, arXiv e-prints, p. arXiv:1910.08034
- Scott N. J., Howell S. B., Horch E. P., Everett M. E., 2018, *PASP*, 130, 054502
- Shporer A., et al., 2017, *ApJ*, 847, L18
- Sinukoff E., et al., 2016, *ApJ*, 827, 78
- Vanderburg A., Johnson J. A., 2014, *PASP*, 126, 948
- Vanderburg A., et al., 2015, *ApJ*, 800, 59
- Vanderburg A., et al., 2016, *ApJS*, 222, 14
- Yu L., et al., 2018, *AJ*, 156, 22
- Zink J. K., et al., 2019, *Research Notes of the American Astronomical Society*, 3, 43
- Zsom A., Seager S., de Wit J., Stamenković V., 2013, *ApJ*, 778, 109

APPENDIX A: APPENDIX

EPIC ID	Campaign	Kp [mag]	g [mag]	r [mag]	i [mag]	B [mag]	V [mag]	J [mag]	H [mag]	K [mag]
249384674 (1)	15	14.794	17.272 ± 0.002	16.044 ± 0.007	14.798 ± 0.004	—	—	12.717 ± 0.023	12.144 ± 0.026	11.911 ± 0.023
249391469	15	14.025	15.765 ± 0.070	14.365 ± 0.010	13.279 ± 0.030	16.515 ± 0.081	14.952 ± 0.045	11.423 ± 0.024	10.756 ± 0.021	10.554 ± 0.024
249557502 (1)	15	16.400	18.463 ± 0.006	17.164 ± 0.003	15.920 ± 0.003	—	—	13.928 ± 0.035	13.293 ± 0.030	12.990 ± 0.036
249826231	15	14.466	16.086 ± 0.030	14.652 ± 0.020	13.772 ± 0.050	16.667 ± 0.060	15.269 ± 0.049	12.042 ± 0.024	11.341 ± 0.022	11.152 ± 0.023
250001426 (2)	15	13.681	15.662 ± 0.010	14.303 ± 0.010	12.832 ± 0.040	16.361 ± 0.140	14.826 ± 0.010	10.658 ± 0.024	10.114 ± 0.022	9.829 ± 0.021
250099723	15	13.803	15.182 ± 0.040	13.839 ± 0.020	13.212 ± 0.070	15.822 ± 0.060	14.400 ± 0.020	11.657 ± 0.027	10.977 ± 0.024	10.797 ± 0.021
201663879 (3)	14	11.932	12.601 ± 0.050	11.924 ± 0.080	11.645 ± 0.020	13.000 ± 0.110	12.172 ± 0.070	10.705 ± 0.026	10.313 ± 0.023	10.223 ± 0.025
201663913 (3)	14	14.451	16.482 ± 0.004	15.126 ± 0.004	14.049 ± 0.004	—	—	12.193 ± 0.027	11.543 ± 0.029	11.333 ± 0.025
201796690 (4)	14	15.798	18.565 ± 0.008	17.082 ± 0.005	15.626 ± 0.004	—	—	13.411 ± 0.032	12.823 ± 0.024	12.508 ± 0.023
248480671	14	12.840	14.457 ± 0.010	13.118 ± 0.010	12.147 ± 0.050	15.127 ± 0.040	13.677 ± 0.050	10.462 ± 0.027	9.796 ± 0.024	9.567 ± 0.021
248558190	14	13.307	14.715 ± 0.060	13.371 ± 0.030	12.703 ± 0.040	15.317 ± 0.060	13.941 ± 0.020	11.194 ± 0.023	10.569 ± 0.023	10.413 ± 0.021
248616368	14	14.132	15.722 ± 0.110	14.387 ± 0.080	13.451 ± 0.080	16.418 ± 0.060	14.932 ± 0.110	11.648 ± 0.023	11.002 ± 0.024	10.789 ± 0.021
248639308	14	14.509	16.142 ± 0.070	14.793 ± 0.030	13.809 ± 0.060	16.783 ± 0.040	15.399 ± 0.020	12.092 ± 0.026	11.457 ± 0.022	11.237 ± 0.026
248775938	14	15.223	16.564 ± 0.020	15.314 ± 0.060	14.649 ± 0.070	17.244 ± 0.106	15.879 ± 0.030	13.087 ± 0.026	12.394 ± 0.023	12.202 ± 0.026
248782482	14	12.585	14.088 ± 0.060	12.745 ± 0.030	11.941 ± 0.050	14.783 ± 0.040	13.358 ± 0.040	10.319 ± 0.021	9.702 ± 0.022	9.488 ± 0.026
246909566	13	17.231	19.506 ± 0.012	17.910 ± 0.007	16.256 ± 0.005	—	—	13.802 ± 0.029	13.210 ± 0.040	12.980 ± 0.031
245944983 (5)	12	12.738	14.154 ± 0.050	12.752 ± 0.040	12.131 ± 0.030	14.725 ± 0.050	13.332 ± 0.020	11.277 ± 0.061	10.618 ± 0.074	10.478 ± 0.061
246074965	12	16.278	18.311 ± 0.007	16.900 ± 0.005	15.407 ± 0.004	—	—	13.177 ± 0.026	12.595 ± 0.030	12.352 ± 0.026
246163416 (2)	12	13.482	15.113 ± 0.090	13.725 ± 0.020	12.783 ± 0.030	15.812 ± 0.050	14.285 ± 0.040	10.995 ± 0.026	10.415 ± 0.026	10.162 ± 0.026
246313886	12	14.481	16.042 ± 0.051	14.523 ± 0.050	13.813 ± 0.069	16.763 ± 0.130	15.163 ± 0.048	12.312 ± 0.031	11.625 ± 0.023	11.427 ± 0.026
246331347 (4)	12	15.459	17.575 ± 0.005	16.129 ± 0.004	15.051 ± 0.005	—	—	13.173 ± 0.026	12.525 ± 0.022	12.304 ± 0.026
246331418 (4)	12	14.472	16.530 ± 0.004	15.096 ± 0.005	14.636 ± 0.002	—	—	12.381 ± 0.024	11.780 ± 0.024	11.571 ± 0.021
246472939	12	14.867	16.409 ± 0.020	14.781 ± 0.040	14.206 ± 0.030	16.926 ± 0.060	15.342 ± 0.070	12.977 ± 0.024	12.231 ± 0.026	12.091 ± 0.026

(1) *gri* photometry extracted from Pan-STARRS DR1.

(2) Close star detected in speckle / AO images.

(3) Signals present at EPIC 201663913 are contamination from the early K-type star EPIC 201663879.

(4) *gri* photometry extracted from SDSS DR15.

(5) Binary star.

Table A1. Photometry of candidate host stars.

EPIC ID	Campaign	Name	Distance [pc]	T _{eff} [K]	Mass [M_{\odot}]	Radius [R_{\odot}]	logg
249384674	15	K2-316	112.84 ± 0.96	3436 ± 3	0.408 ± 0.005	0.379 ± 0.003	4.891 ± 0.002
249391469	15	–	101.56 ± 0.40	3503 ± 63	0.337 ± 0.079	0.567 ± 0.018	4.447 ± 0.130
249557502	15	K2-317	177.08 ± 3.34	3387 ± 5	0.403 ± 0.006	0.379 ± 0.006	4.885 ± 0.011
249826231	15	K2-318	148.49 ± 0.99	3851 ± 83	0.561 ± 0.050	0.552 ± 0.017	4.701 ± 0.070
250001426 (1)	15	–	-----	-----	-----	-----	-----
250009723	15	–	143.29 ± 0.58	4176 ± 78	0.603 ± 0.017	0.576 ± 0.007	4.696 ± 0.012
201663879 (2)	14	K2-319	210.56 ± 1.37	5440 ± 115	0.954 ± 0.055	0.898 ± 0.013	4.512 ± 0.055
201663913 (2,3)	14	–	215.94 ± 2.19	3874 ± 72	0.649 ± 0.016	0.678 ± 0.020	4.588 ± 0.026
201796690	14	K2-320	109.07 ± 1.04	3157 ± 7	0.117 ± 0.011	0.300 ± 0.003	4.550 ± 0.036
248480671	14	K2-321	77.86 ± 0.32	3855 ± 65	0.599 ± 0.027	0.583 ± 0.016	4.683 ± 0.042
248558190	14	K2-322	123.86 ± 0.31	4141 ± 96	0.630 ± 0.033	0.602 ± 0.013	4.677 ± 0.041
248616368	14	K2-323	118.72 ± 0.55	3710 ± 118	0.478 ± 0.089	0.549 ± 0.024	4.630 ± 0.127
248639308	14	K2-324	137.18 ± 1.60	3752 ± 57	0.517 ± 0.041	0.505 ± 0.012	4.743 ± 0.057
248775938	14	–	305.58 ± 6.75	4663 ± 144	0.625 ± 0.023	0.608 ± 0.014	4.665 ± 0.019
248782482	14	–	62.16 ± 0.16	3852 ± 52	0.518 ± 0.029	0.503 ± 0.008	4.749 ± 0.037
246909566	13	–	98.51 ± 1.43	3067 ± 5	0.121 ± 0.007	0.236 ± 0.004	4.772 ± 0.027
245944983 (4)	12	–	-----	-----	-----	-----	-----
246074965 (3)	12	K2-325	111.98 ± 1.02	3287 ± 67	0.274 ± 0.008	0.298 ± 0.009	4.840 ± 0.026
246163416 (1)	12	–	-----	-----	-----	-----	-----
246313886	12	–	156.46 ± 0.95	3949 ± 54	0.523 ± 0.015	0.503 ± 0.005	4.753 ± 0.012
246331347	12	–	190.96 ± 2.29	3408 ± 17	0.245 ± 0.027	0.516 ± 0.009	4.399 ± 0.062
246331418	12	–	157.71 ± 1.06	4408 ± 5	0.276 ± 0.006	0.427 ± 0.004	4.617 ± 0.013
246472939	12	K2-326	284.58 ± 3.37	3924 ± 51	0.507 ± 0.051	0.688 ± 0.014	4.462 ± 0.059

(1) Close blended source detected in speckle / AO images. Unreliable stellar parameters.

(2) Signals present at EPIC 201663913 are contamination from the early K-type star EPIC 201663879.

(3) Stellar parameters from Dressing (2019).

(4) Binary star. Unreliable stellar parameters.

Table A2. Candidate hosts stars parameters.

Candidate	C	Name	P_{orb} [d]	a [AU]	R_p [R_{\oplus}]	T_{eq} [K]	Epoch (BKJD) [d]	i [deg]	b	Transit Depth [mag]	SNR
249384674 b	15	K2-316 b	1.133 ± 0.001	$0.0147^{+0.0010}_{-0.0031}$	$1.33^{+0.10}_{-0.09}$	841^{+105}_{-54}	3158.605	$87.02^{+2.19}_{-3.98}$	$0.43^{+0.32}_{-0.30}$	0.00104 ± 0.00002	15.5
249384674 c	15	K2-316 c	5.260 ± 0.007	$0.0582^{+0.0081}_{-0.0122}$	$1.83^{+0.13}_{-0.12}$	423^{+53}_{-26}	3161.123	$89.31^{+0.49}_{-1.06}$	$0.40^{+0.34}_{-0.28}$	0.00270 ± 0.00006	14.8
249391469 b (1)	15	–	1.075 ± 0.003	–	–	–	3158.860	–	–	0.00095 ± 0.00001	28.3
249557502 b	15	K2-317 b	6.220 ± 0.007	$0.0542^{+0.0065}_{-0.0103}$	$2.93^{+0.19}_{-0.17}$	432^{+48}_{-24}	3161.132	$89.22^{+0.54}_{-0.93}$	$0.43^{+0.29}_{-0.28}$	0.00129 ± 0.00014	13.6
249826231 b	15	K2-318 b	7.010 ± 0.007	$0.0911^{+0.0140}_{-0.0185}$	1.66 ± 0.13	456^{+55}_{-32}	3164.194	$89.38^{+0.44}_{-0.76}$	$0.40^{+0.29}_{-0.27}$	0.00092 ± 0.00002	11.7
250001426 b (2)	15	–	$1.705^{+0.004}_{-0.003}$	–	–	–	3159.286	–	–	0.00056 ± 0.00001	17.1
250009723 b	15	–	$17.920^{+0.013}_{-0.014}$	$0.1417^{+0.0158}_{-0.0285}$	2.07 ± 0.09	407^{+48}_{-23}	3170.786	$89.57^{+0.31}_{-0.50}$	$0.40^{+0.29}_{-0.28}$	0.00097 ± 0.00004	11.8
201663879 b (3)	14	K2-319 b	$26.680^{+0.002}_{-0.003}$	$0.1516^{+0.0115}_{-0.0258}$	$2.79^{+0.11}_{-0.10}$	641^{+61}_{-31}	3082.592	$89.45^{+0.40}_{-0.66}$	$0.35^{+0.28}_{-0.24}$	0.00090 ± 0.00001	19.1
201663879 c (3)	14	–	$35.621^{+0.003}_{-0.002}$	$0.3501^{+0.0449}_{-0.0648}$	$1.89^{+0.14}_{-0.13}$	420^{+47}_{-27}	3078.974	$89.77^{+0.17}_{-0.31}$	$0.35^{+0.31}_{-0.26}$	0.00045 ± 0.00002	9.4
201796690 b	14	K2-320 b	1.995 ± 0.001	$0.0142^{+0.0026}_{-0.0050}$	$2.62^{+0.23}_{-0.15}$	698^{+87}_{-57}	3075.602	$87.84^{+1.41}_{-1.97}$	$0.49^{+0.25}_{-0.30}$	0.00606 ± 0.00006	17.2
248480671 b	14	K2-321 b	2.298 ± 0.001	$0.0410^{+0.0035}_{-0.0048}$	$1.95^{+0.10}_{-0.12}$	701^{+45}_{-30}	3076.170	$88.94^{+0.73}_{-1.12}$	$0.28^{+0.24}_{-0.19}$	0.00120 ± 0.00001	27.9
248558190 b	14	K2-322 b	8.205 ± 0.003	$0.0594^{+0.0174}_{-0.0221}$	$1.92^{+0.19}_{-0.18}$	635^{+165}_{-78}	3081.022	$88.15^{+1.11}_{-2.01}$	$0.68^{+0.21}_{-0.33}$	0.00077 ± 0.00002	19.8
248616368 b	14	K2-323 b	24.930 ± 0.006	$0.1275^{+0.0055}_{-0.0072}$	$2.10^{+0.09}_{-0.11}$	318^{+24}_{-43}	3081.251	$89.88^{+1.08}_{-1.29}$	$0.14^{+0.11}_{-0.09}$	0.00286 ± 0.00011	19.3
248639308 b	14	K2-324 b	3.262 ± 0.001	$0.0331^{+0.0037}_{-0.0066}$	$2.43^{+0.15}_{-0.13}$	707^{+83}_{-38}	3076.146	$88.33^{+1.06}_{-1.84}$	$0.42^{+0.28}_{-0.25}$	0.00216 ± 0.00002	94.2
248775938 b	14	–	1.754 ± 0.001	$0.0365^{+0.0038}_{-0.0053}$	$5.06^{+0.49}_{-0.44}$	873^{+75}_{-54}	3074.851	$88.26^{+1.17}_{-1.73}$	$0.39^{+0.27}_{-0.26}$	0.00568 ± 0.00003	10.5
248782482 b	14	–	$16.222^{+0.012}_{-0.014}$	$0.0999^{+0.0124}_{-0.0229}$	$1.28^{+0.11}_{-0.09}$	417^{+58}_{-24}	3080.007	$89.49^{+0.37}_{-0.72}$	$0.39^{+0.33}_{-0.27}$	0.00056 ± 0.00002	10.2
246909566 b	13	–	$1.925^{+0.003}_{-0.004}$	$0.0251^{+0.0048}_{-0.0047}$	$1.07^{+0.09}_{-0.08}$	452^{+48}_{-38}	2988.974	$89.13^{+0.61}_{-1.02}$	$0.36^{+0.28}_{-0.24}$	0.00216 ± 0.00002	10.8
245944983 b (4)	12	–	5.138 ± 0.002	–	–	–	2910.267	–	–	0.00073 ± 0.00001	9.6
246074965 b	12	K2-325 b	$6.930^{+0.004}_{-0.003}$	$0.0419^{+0.0046}_{-0.0058}$	$2.20^{+0.14}_{-0.15}$	423^{+33}_{-21}	2910.818	$89.37^{+0.40}_{-0.68}$	$0.34^{+0.26}_{-0.22}$	0.00732 ± 0.00011	15.8
246163416 b (2)	12	–	$0.877^{+0.003}_{-0.003}$	–	–	–	2905.852	–	–	0.00050 ± 0.00001	11.2
246313886 b	12	–	1.827 ± 0.002	$0.0187^{+0.0038}_{-0.0043}$	$0.99^{+0.11}_{-0.09}$	986^{+138}_{-88}	2906.474	$87.19^{+2.07}_{-3.88}$	$0.43^{+0.32}_{-0.31}$	0.00035 ± 0.00002	10.0
246331347 b	12	–	1.082 ± 0.001	$0.0162^{+0.0027}_{-0.0034}$	$2.22^{+0.21}_{-0.18}$	928^{+119}_{-68}	2906.474	$86.19^{+2.59}_{-5.24}$	$0.46^{+0.32}_{-0.30}$	0.00162 ± 0.00003	15.8
246331418 b	12	–	3.350 ± 0.002	$0.0266^{+0.0064}_{-0.0060}$	0.97 ± 0.11	851^{+117}_{-86}	2908.005	$88.21^{+1.30}_{-2.36}$	$0.44^{+0.31}_{-0.31}$	0.00063 ± 0.00003	10.5
246331418 c	12	–	9.320 ± 0.001	$0.0724^{+0.0123}_{-0.0178}$	$1.43^{+0.13}_{-0.14}$	516^{+78}_{-39}	2911.661	$89.30^{+0.49}_{-0.92}$	$0.44^{+0.32}_{-0.29}$	0.00109 ± 0.00005	10.7
246472939 b	12	K2-326 b	$1.256^{+0.001}_{-0.002}$	$0.0198^{+0.0036}_{-0.0041}$	$2.28^{+0.18}_{-0.18}$	1114^{+138}_{-90}	2906.045	$85.63^{+2.87}_{-4.24}$	$0.48^{+0.26}_{-0.29}$	0.00100 ± 0.00003	11.4

(1) False positive. The signal comes from Gaia DR2 6239523158128298496.

(2) Close blended source detected in speckle / AO images. Unreliable stellar and therefore planetary parameters.

(3) Signal from an early K-type star.

(4) Candidate signal from a binary star.

Table A3. Parameters of planetary candidates presented in this work.

This paper has been typeset from a T_EX/L^AT_EX file prepared by the author.

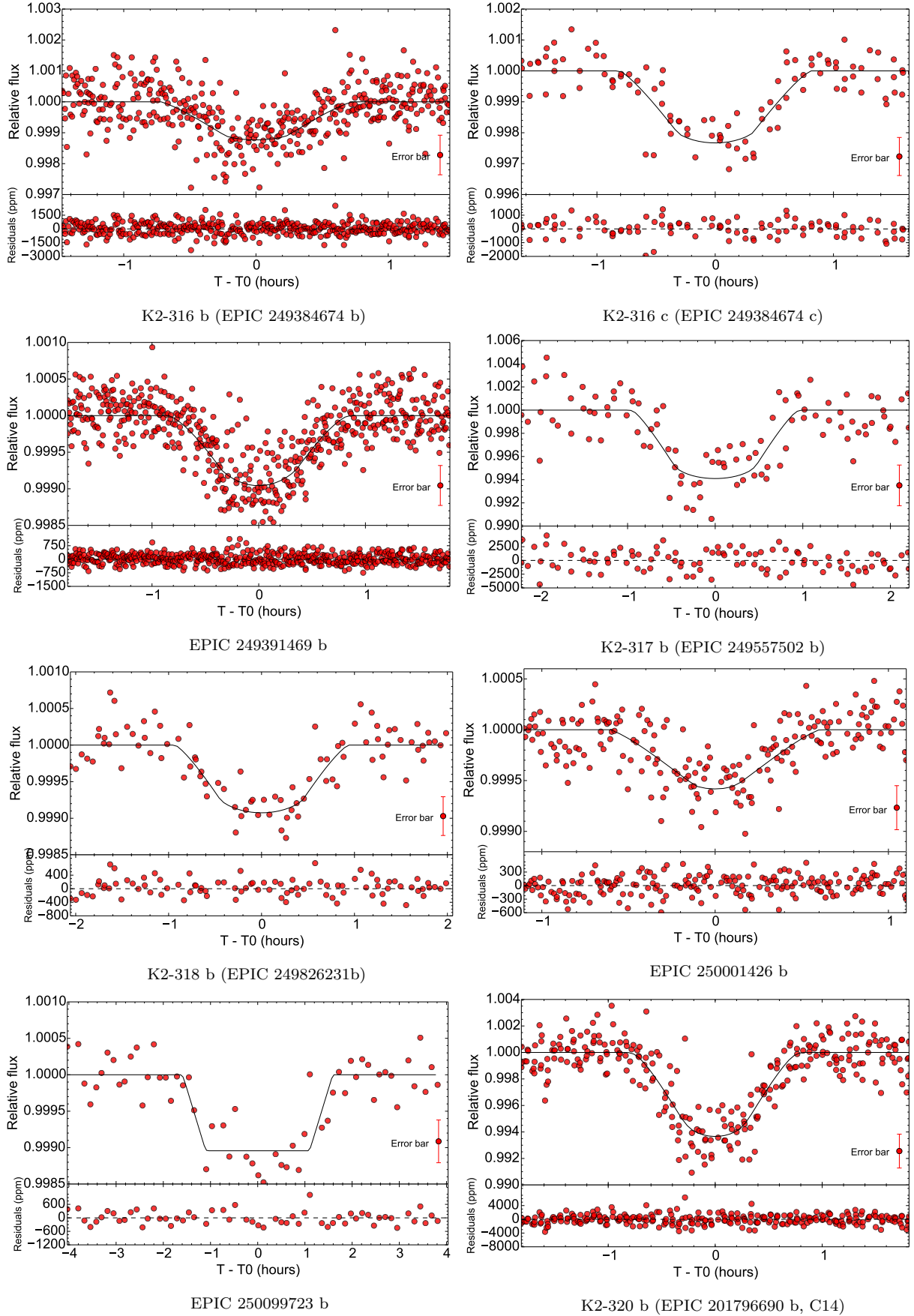


Figure A1. Phase-folded transits and best fit for planetary candidates of campaign 15 and 14 (K2-320 b).

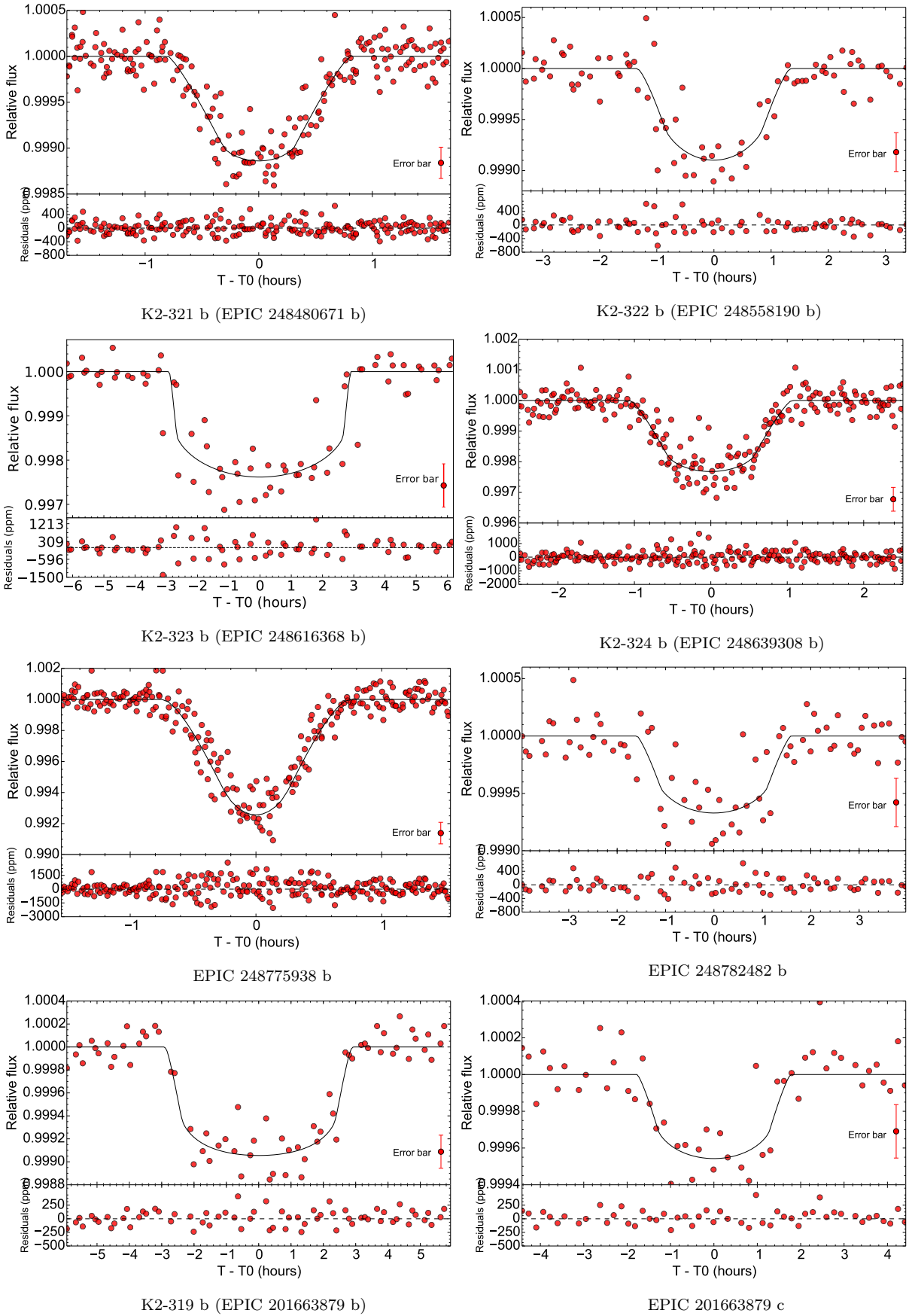
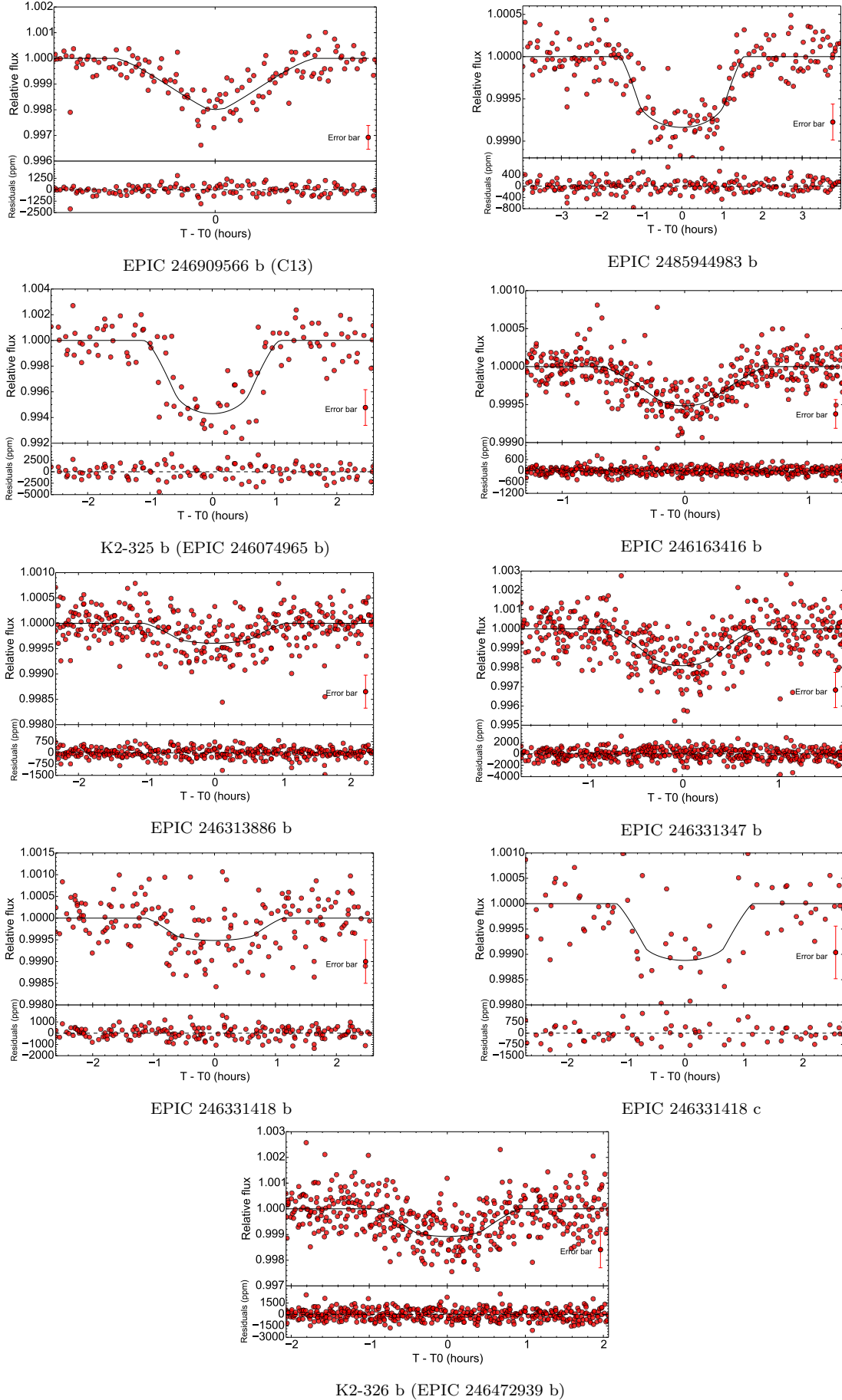


Figure A2. Phase-folded transits and best fit for planetary candidates of campaign 14.



MNRAS 000, 1–20 (2024) **Figure A3.** Phase-folded transits for candidates of campaign 12 and 13 (EPIC 246909566b).

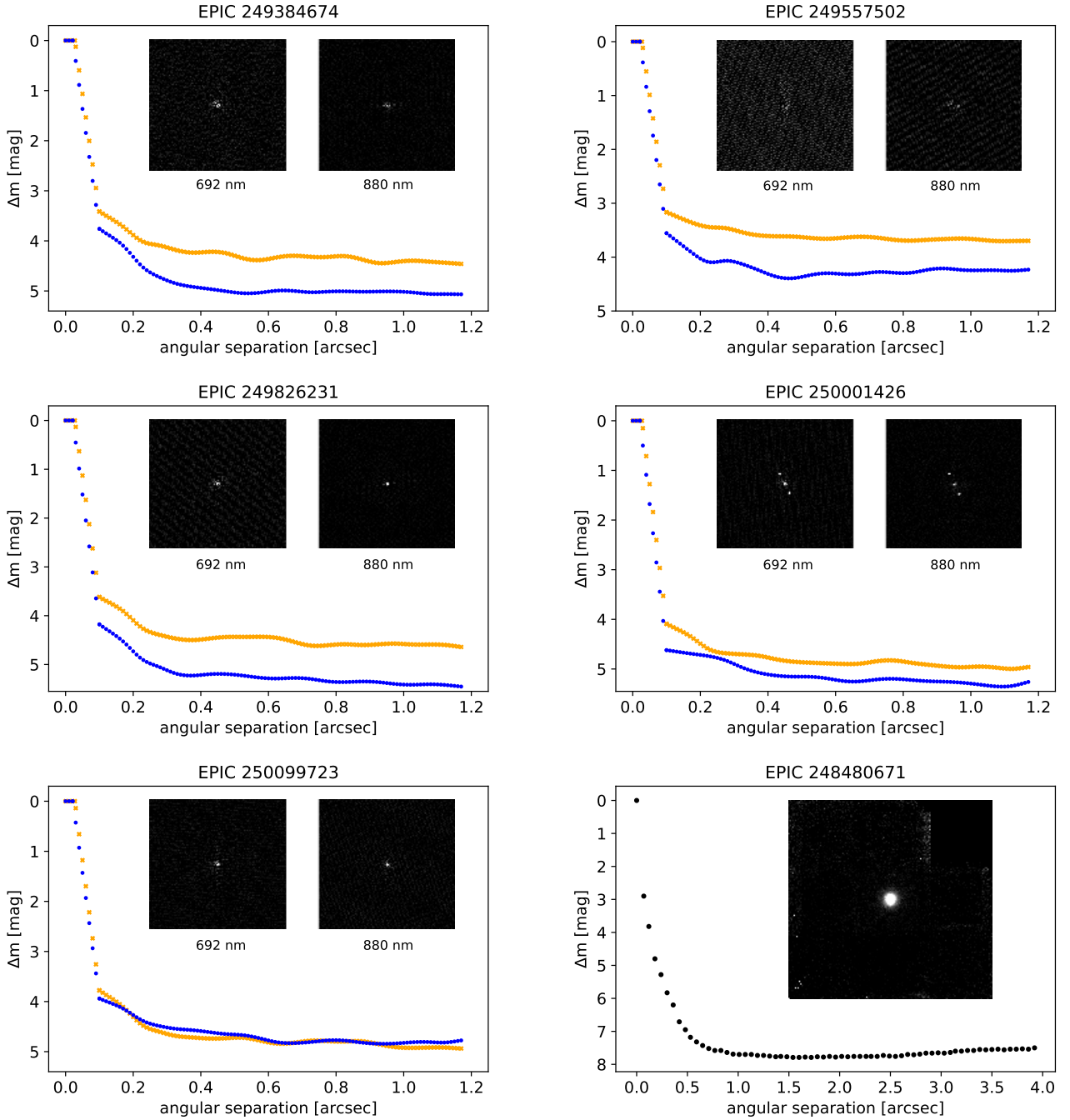


Figure A4. Speckle images and background plots for 5 stars from C15 and an AO image for EPIC 248480671 (C14). The 5 images from C15 stars have been acquired at GeminiS-8m telescope at 880 nm (orange crosses) and 692 nm (blue dots) in a field of 3 x 3 arc seconds. The AO image for EPIC 248480671, was acquired with NIRC2 at Keck-10m telescope (field 8 x 8 arc seconds).

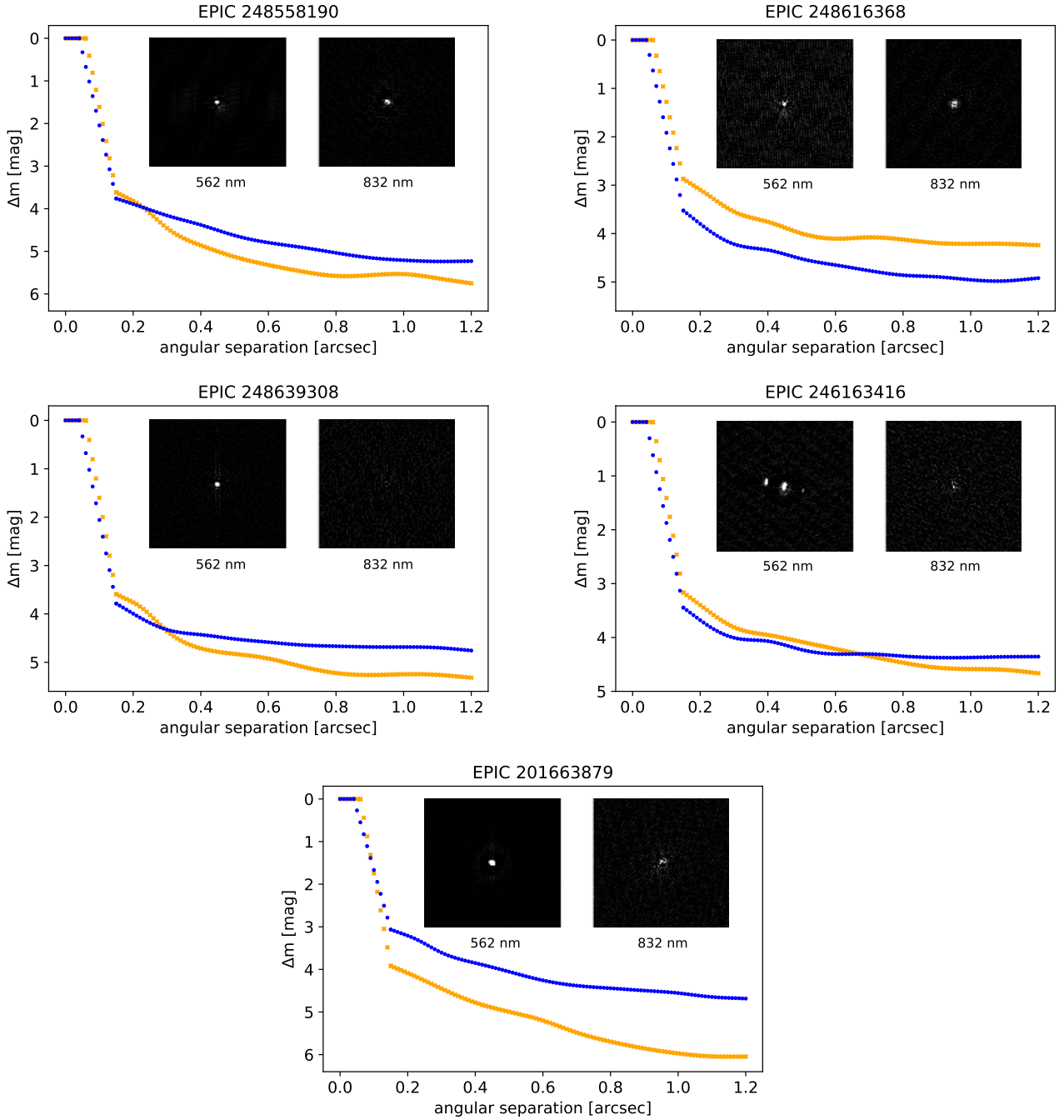


Figure A5. Speckle images and background plot for 4 stars from C14 and 1 from C12 (EPIC 246163416). All images were acquired with NESSI instrument at WIYN-3.5m telescope at 832 nm (orange crosses) and 562 nm (blue dots). The field of the images is 4.65 x 4.65 arc seconds.

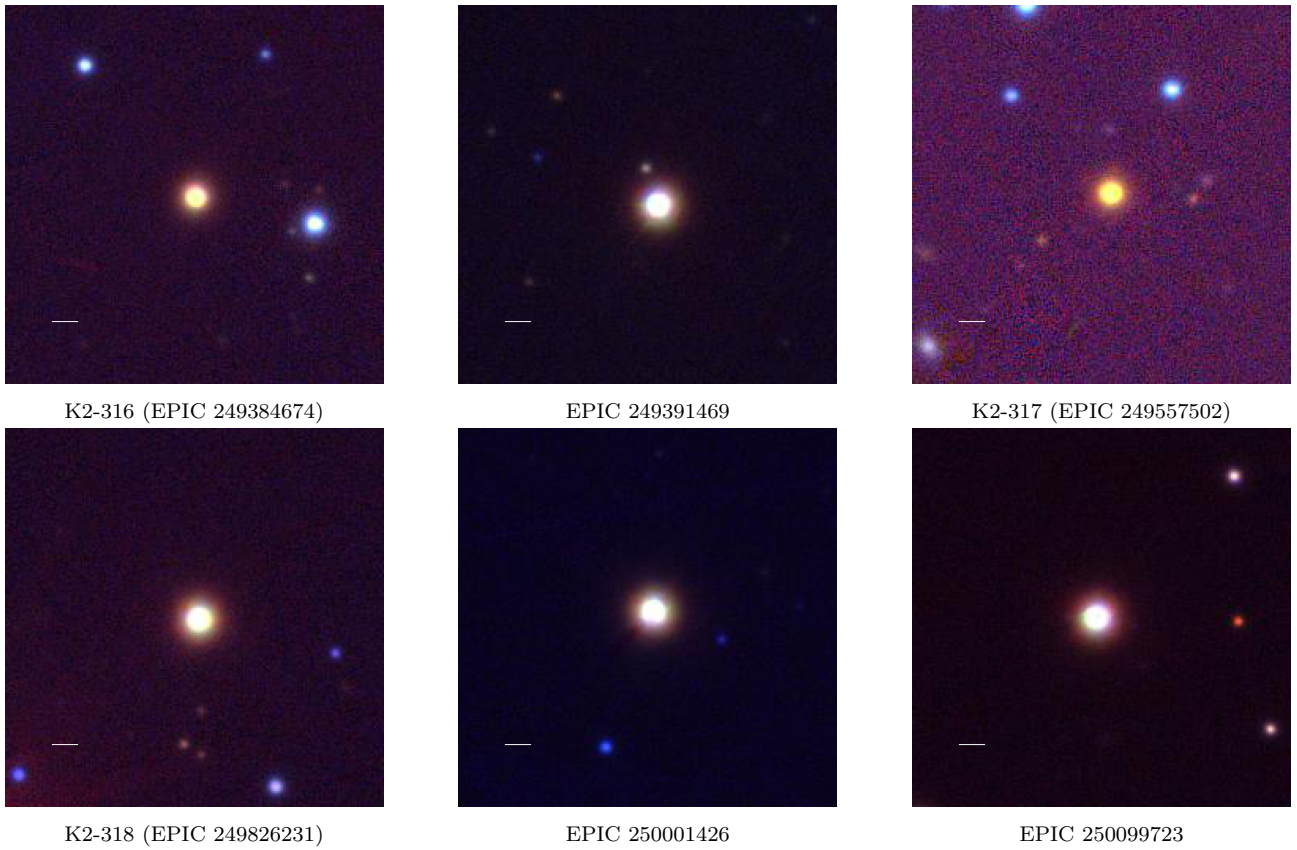


Figure A6. Panstarrs y/i/g stacked images of planet candidate hosts from campaign 15. Image size is 60.00 arc seconds. North up, East left. Straight white lines indicate the 3.98 arc seconds size of the Kepler pixel.

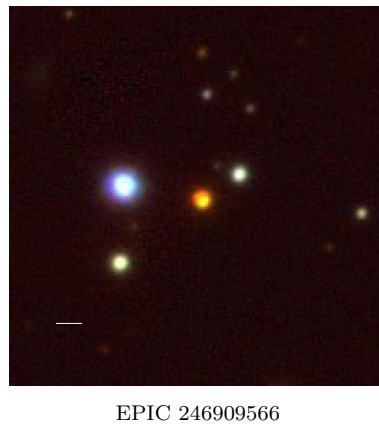


Figure A7. Panstarrs y/i/g stacked images of planet candidate hosts from campaign 13. Image size is 60.00 arc seconds. North up, East left. Straight white line indicate the 3.98 arc seconds size of the Kepler pixel.

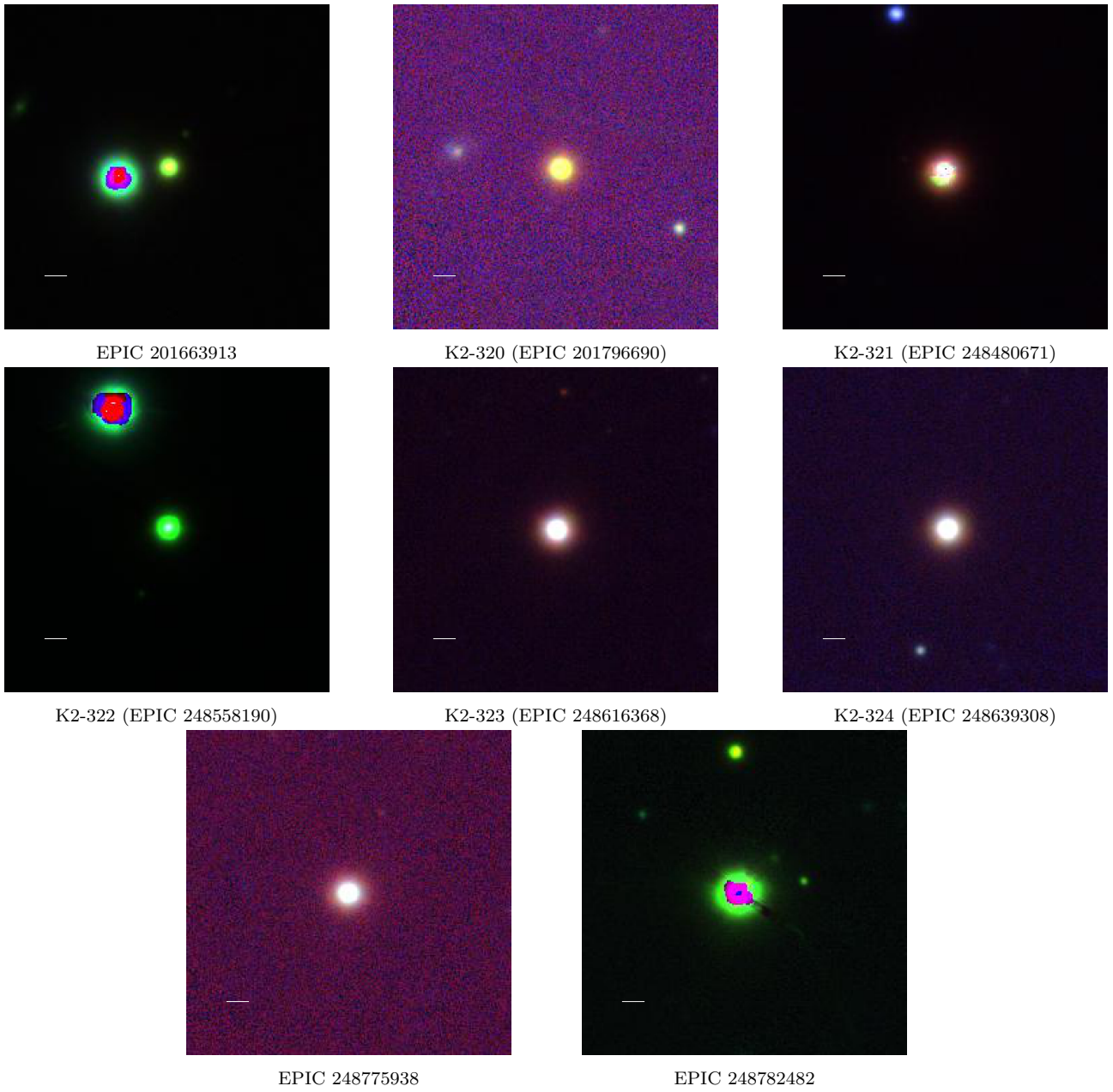


Figure A8. Panstarrs y/i/g stacked images of planet candidate hosts from campaign 14. Image size is 60.00 arc seconds. North up, East left. Straight white lines indicate the 3.98 arc seconds size of the Kepler pixel.



Figure A9. Panstarrs *y/i/g* stacked images of planet candidate hosts from campaign 12. Image size is 60.00 arc seconds. North up, East left. Straight white lines indicate the 3.98 arc seconds size of the Kepler pixel.